Acta Pharmaceutica Sinica B 2021;11(2):572–587

Chinese Pharmaceutical Association
Institute of Materia Medica, Chinese Academy of Medical Sciences

Acta Pharmaceutica Sinica B

www.elsevier.com/locate/apsb
www.sciencedirect.com

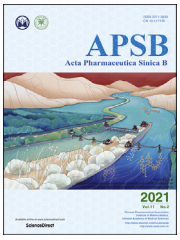

ORIGINAL ARTICLE

Genome mining combined metabolic shunting and OSMAC strategy of an endophytic fungus leads to the production of diverse natural products

Qian Wei[a,†], Jian Bai[a,†], Daojiang Yan[a], Xiuqi Bao[a], Wenting Li[b], Bingyu Liu[a], Dan Zhang[a], Xiangbing Qi[b], Dequan Yu[a], Youcai Hu[a,*]

[a]*State Key Laboratory of Bioactive Substance and Function of Natural Medicines, Institute of Materia Medica, Chinese Academy of Medical Sciences & Peking Union Medical College, Beijing 100050, China*
[b]*National Institute of Biological Sciences, Beijing 102206, China*

Received 9 May 2020; received in revised form 27 June 2020; accepted 21 July 2020

KEY WORDS

Endophytic fungi;
Penicillium dangeardii;
Genome mining;
Silent gene cluster;
Azaphilones;
Trimers;
Metabolic shunting

Abstract Endophytic fungi are promising producers of bioactive small molecules. Bioinformatic analysis of the genome of an endophytic fungus *Penicillium dangeardii* revealed 43 biosynthetic gene clusters, exhibited its strong ability to produce numbers of secondary metabolites. However, this strain mainly produce rubratoxins alone with high yield in varied culture conditions, suggested most gene clusters are silent. Efforts for mining the cryptic gene clusters in *P. dangeardii*, including epigenetic regulation and one-strain-many-compounds (OSMAC) approach were failed probably due to the high yield of rubratoxins. A metabolic shunting strategy by deleting the key gene for rubratoxins biosynthesis combining with optimization of culture condition successfully activated multiple silent genes encoding for other polyketide synthases (PKSs), and led to the trace compounds detectable. As a result, a total of 23 new compounds including azaphilone monomers, dimers, trimers with unprecedented polycyclic bridged heterocycle and spiral structures, as well as siderophores were identified. Some compounds showed significant cytotoxicities, anti-inflammatory or antioxidant activities. The attractive dual PKSs gene clusters for azaphilones biosynthesis were mined by bioinformatic analysis and overexpression of a pathway specific transcription factor. Our work therefor provides an efficient approach to mine the chemical diversity of endophytic fungi.

*Corresponding author. Tel.: +86 10 83162679; fax: +86 10 63017757.
E-mail address: huyoucai@imm.ac.cn (Youcai Hu).
[†]These authors contributed equally to this work.
Peer review under responsibility of Institute of Materia Medica, Chinese Academy of Medical Sciences and Chinese Pharmaceutical Association.

https://doi.org/10.1016/j.apsb.2020.07.020

1. Introduction

Endophytic fungi, which live inside plants interacting with the host and promoting plant growth, have been proved to be promising producer of secondary metabolites with novel structures and a remarkable range of activities such as antibacterial, insecticidal, anticancer, plant hormone and antioxidant[1,2]. For instance, *Taxomyces andreanae*, isolated from the phloem of *Taxus brevifolia*, could produce taxol as an anti-tumor agent in breast and ovarian cancers[3]. However, advances in genome sequencing and bioinformatics revealed that fungi with many biosynthetic gene clusters have far greater ability to encode secondary metabolites than which were produced under standard laboratory culture conditions. So various genome mining strategies have been applied to activate silent gene clusters for the biosynthesis of natural products[4,5], including one-strain-many-compounds (OSMAC)[6,7], co-cultivation[8], chemical epigenetics[9], ribosome engineering[10], epigenetic modification[11,12], overexpression of transcription factor[13] and heterologous expression[14], and achieved amazing results.

Penicillium dangeardii is a filamentous fungus isolated from a toxic plant *Lysidice rhodostegia* (Leguminosae sp.)[15]. Investigation on its chemical compositions mainly led to the isolation of large anhydrides such as rubratoxins A–C (**1**–**3**, Fig. 1A)[16,17] and penicillactones A–C[15]. Due to the highly oxidized complex structure and bioactivity, the biosynthesis pathway of rubratoxins A and B has been elucidated[18]. However, analysis of genomic information of *P. dangeardii* revealed 43 gene clusters responsible for natural products biosynthesis, which are significantly more than the number of above known anhydrides metabolites, suggesting that most gene clusters are cryptic.

To activate the cryptic gene clusters in *P. dangeardii*, OSMAC strategy and epigenetic regulation[11] were firstly applied, respectively. Unfortunately, it failed probably due to the super-high yield of rubratoxins (0.65 g/L). Alternatively, a metabolic shunting strategy based on deletion of the key gene for rubratoxins biosynthesis and optimization of culture condition successfully activated multiple cryptic gene clusters involved in the biosynthesis of polyketides, which resulted in the isolation of a large number of new metabolites, including azaphilone monomers, dimers, and trimers featuring unprecedented polycyclic bridged heterocycle and spiral structures, as well as siderophores. All isolated compounds were evaluated for their cytotoxicities, anti-inflammatory and antioxidant activities, and the gene clusters for azaphilones biosynthesis were characterized.

2. Results and discussion

2.1. Bioinformatic analysis of genome of P. dangeardii

Bioinformatic analysis of the genome sequence from *P. dangeardii* showed 43 gene clusters that encode biosynthesis of natural products, including 22 polyketide synthases (PKSs), 8 nonribosomal peptide synthases (NRPSs), 8 PKSs/NRPSs hybrids, and 5 terpene synthases (TSs; Supporting Information Tables

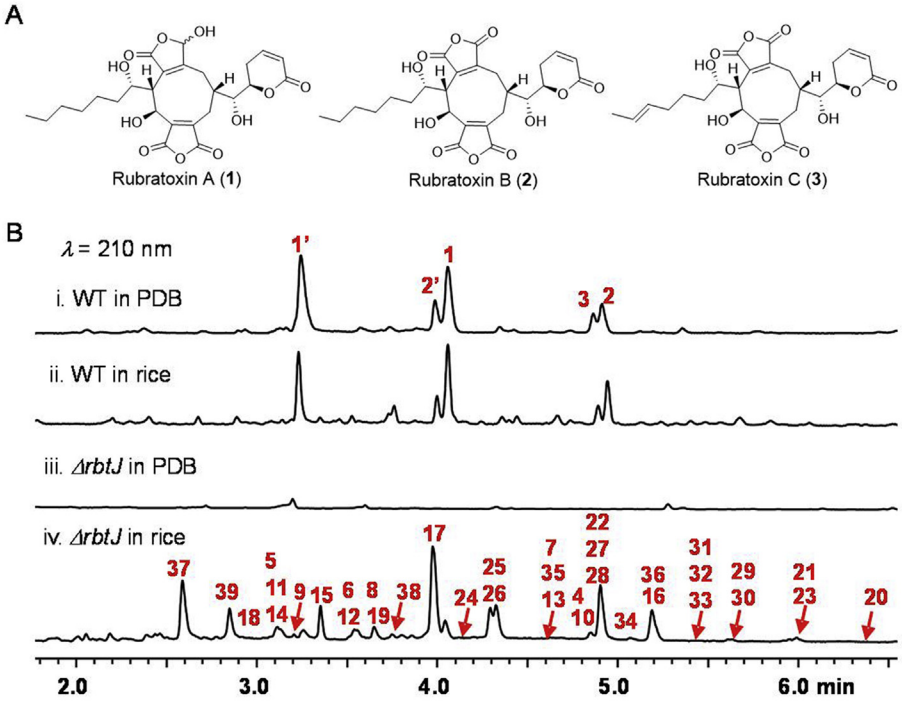

Figure 1 Analyses of metabolites from *P. dangeardii*. (A) The structures of anhydrides. (B) LC–MS analyses of crude extracts from wild type (WT) and *ΔrbtJ* mutant strain fermented in PDB and rice culture media. The number on the peaks corresponds to the products shown in Figs. 1A and 2. The anhydrides are partially present as diacids (labeled 1′ and 2′) in aqueous solvent.

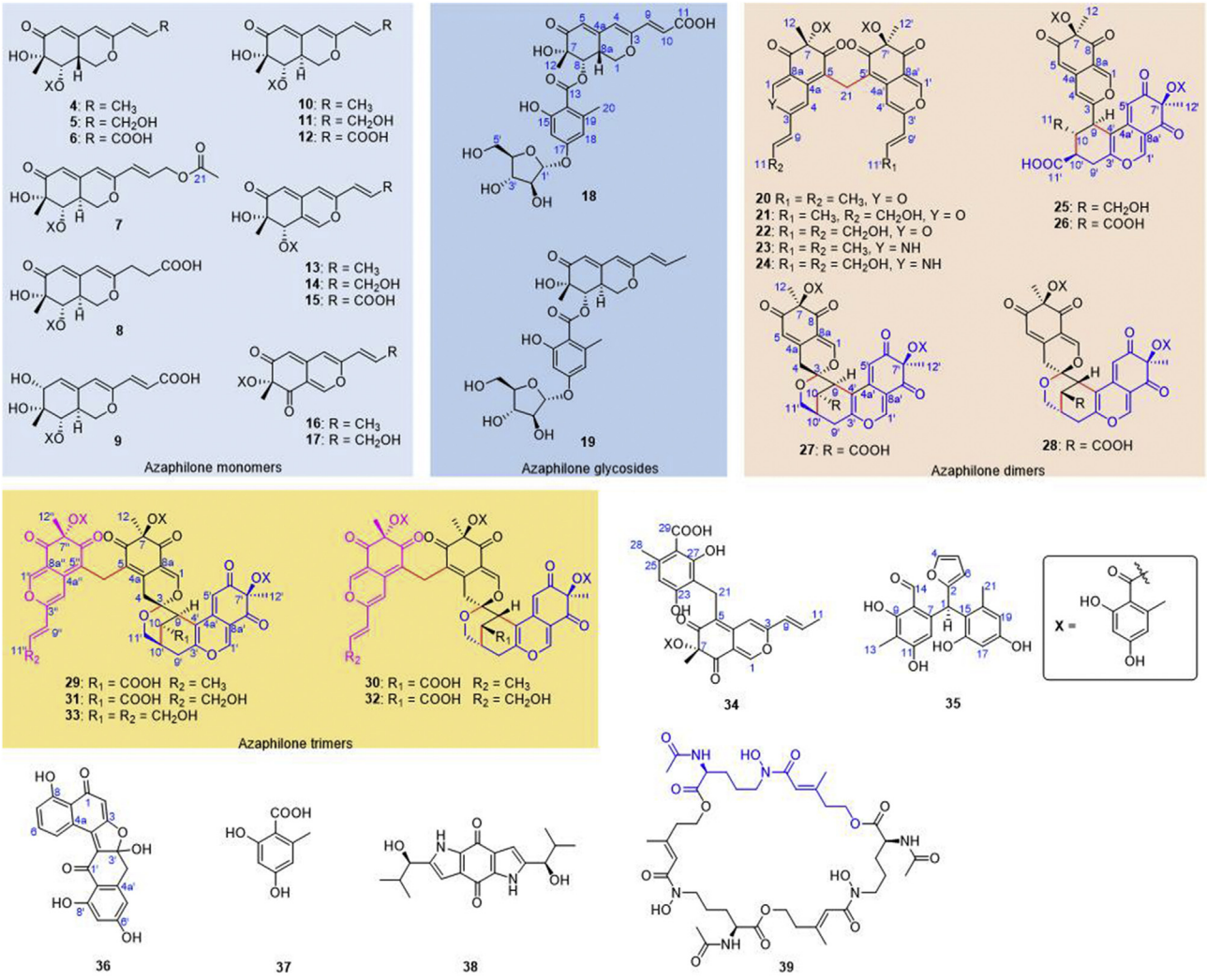

Figure 2 Compounds purified from *P. dangeardii ΔrbtJ* mutant strain.

S1−S3), which far exceeds the number of the predominant anhydrides rubratoxins A−C (Fig. 1A). This indicated that the title strain possesses potential to produce more diverse natural compounds.

2.2. *OSMAC strategy and epigenetic modification applied on P. dangeardii*

To develop its potential for biosynthesis of pleiotropic second metabolites, an OSMAC strategy was applied, where *P. dangeardii* was cultured in different media, including potato dextrose agar (PDA), potato dextrose broth (PDB), Czapek concentrate yeast extract (CY), yeast extract glucose (YG), yeast extract malt extract glucose (YMEG), and rice (Secition 4.1. Strains and cultivation conditions). However, no additional metabolites except rubratoxins were produced, indicated by LC–MS analysis (Supporting Information Fig. S1). Moreover, deletion of the four epigenetic regulation genes separately did not lead to the generation of any new products (data not show). With the high yield of rubratoxins in wild type or mutant strains, we believe that acetyl CoA, the starting unit for polyketide synthase was largely consumed by rubratoxins biosynthesis, which inhibits the biosynthesis of other polyketides and makes efforts to activate cryptic gene cluster unsuccessful. In addition, the presence of high yield of rubratoxins in *P. dangeardii* also leads to the trace secondary metabolites undetectable. Therefore, a strategy based on inhibition of rubratoxins production was believed to be efficient for mining the chemical diversity in *P. dangeardii*.

2.3. *Combinational genome mining leads to the production of abundant metabolites*

To inhibit the production of rubratoxins, the gene *rbtJ* encoding PKS for rubratoxins biosynthesis was deleted, to give a mutant strain *ΔrbtJ*, which was screened for appropriate culture media. Among the screening rice, PDA, PDB, CY, YG, and YMEG media, rice medium was found to be a perfect medium for strain *ΔrbtJ*, where abundant metabolites were detectable through LC–MS analysis (Fig. 1B and Supporting Information Fig. S2). Comprehensive reverse transcription-PCR (RT-PCR) analysis of all 43 core biosynthetic genes exhibited that most core genes in the wild type showed weak to no expression except for the PKS gene for biosynthesis of rubratoxins in contig 20, while inhibiting the production of rubratoxins resulted in significantly increased expression of four additional PKS genes in contigs 4 and 60 (Supporting Information Fig. S3). Therefore, the combinational

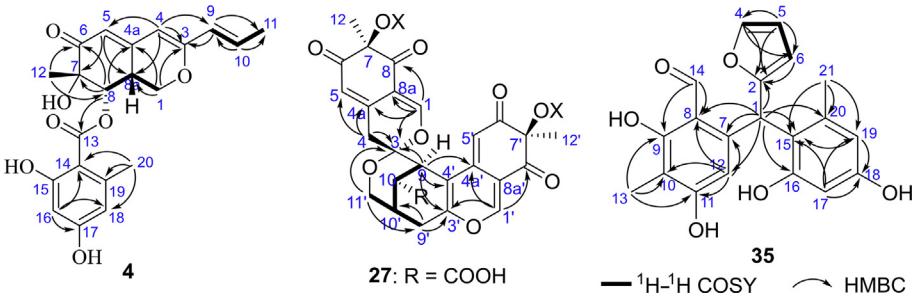

Figure 3 $^{1}H-^{1}H$ COSY and key HMBC correlations of compounds **4**, **27**, and **35**.

strategy applied here successfully up-regulated the expression of multiple cryptic genes encoding for PKSs and led to the pleiotropic production of secondary metabolism.

To identify the newly produced compounds in the *ΔrbtJ* strain, a large-scale fermentation (13 kg) in rice was carried out, following by various chromatography, which resulted in the isolation of a total of 36 compounds from part fractions (Fig. 2), of which 23 compounds possess new structure, including 9 azaphilone monomers (**4**−**9**, **18**−**19** and **34**), 8 azaphilone dimers (**20**−**25**, **27** and **28**), 5 azaphilone trimers (**29**−**33**), and 1 unclassified polyketide (**35**), along with 13 known ones including polyketides Sch 725680 (**10**)[19], pinophilin B (**11**)[20], pinazaphilone B (**12**)[21], Sch 1385568 (**13**)[22], talaraculone F (**14**)[23], (+)-mitorubrinic acid B (**15**)[24], (−)-mitorubrin (**16**)[25,26], (−)-mitorubrinol (**17**)[25], diazaphilonic acid (**26**)[27,28], (±)-asperlones A (**36**)[29] and orsellinic acid (**37**)[30], alkaloid terreusinone (**38**)[31], and a siderophore desferritriacetylfusigen (**39**)[32,33]. Remarkably, three types of novel azaphilones polymers were discovered for the first time, including 5 unusual methylene-bridged azaphilone dimers (**20**−**24**), 2 rare spiro-polycyclic azaphilone dimers (**27** and **28**), and 5 unprecedented azaphilone trimers (**29**−**33**) featuring both methylene and polycyclic bridged heterocycle and spiral structures, tetrahydro-3-oxaspiro[bicyclo[3.3.1]nonane-2,2′-pyran] core.

Compound **4** was isolated as a yellow amorphous powder. The molecular formula $C_{21}H_{22}O_7$ was determined according to its high resolution ESI MS (HR-ESI-MS) spectrum ($[M+H]^+$, *m/z* 387.1438; Calcd. for $C_{21}H_{23}O_7$, 387.1438) combined with the ^{1}H NMR and ^{13}C NMR data (Supporting Information Tables S4 and S5). IR spectrum showed the presence of hydroxy (3355 cm^{-1}), conjugated carbonyl (1645 cm^{-1}), and phenyl (1583 and 1447 cm^{-1}) groups. The ^{1}H NMR and ^{13}C NMR spectra of **4** showed two aromatic proton signals at δ_H 6.11 (s, 2H), a methyl protons at δ_H 2.12 (s, 3H), two phenolic hydroxy protons at δ_H 9.96 (s), 10.63 (s), a conjugated carbonyl carbon at δ_C 169.0, and six aromatic carbon signals in the region of δ_C 100.3−161.1, indicating the existence of 2,4-dihydroxy-6-methyl benzoic acid (orsellinic acid) moiety[19,21]. In addition, the NMR data also displayed resonances attributable to a conjugated ketene at δ_C 198.5 (C-6), two olefinic protons at δ_H 5.72 (d, J = 2.1 Hz, H-5), 5.77 (s, H-4), two *E*-configured olefinic protons at δ_H 6.33 (dq, J = 15.5, 6.9 Hz, H-10), 6.01 (dd, J = 15.5, 1.6 Hz, H-9), two methyl groups at δ_H 1.81 (d, J = 6.9, 1.6 Hz, H_3-11), 1.33 (s, H_3-12), an oxygenated methylene at δ_H 3.75 (dd, J = 12.9, 10.6 Hz, H-1a), 4.51 (dd, J = 10.6, 5.2 Hz, H-1b), δ_C 66.8 (C-1), an oxygen-bearing methine at δ_H 5.60 (d, J = 2.8 Hz, H-8), δ_C 77.2 (C-8), a methine at δ_H 3.43 (m, H-8a), δ_C 35.7 (C-8a), an alcoholic hydroxy proton at δ_H 5.36 (s, 7-OH), and three quaternary carbons at δ_C 158.5 (C-3), 149.1 (C-4a), 74.8 (C-7).

Analysis of the $^{1}H-^{1}H$ COSY NMR data of **4** identified the C-1/C-8a/C-8 and C-9/C-10/C-11 moieties (Fig. 3). HMBC correlations from olefin proton H-5 to C-7/C-8a, from oxygenated methine proton H-8 to ketone carbonyl C-6/C-4a/C-7, and from Me-12 to C-6/C-7/C-8 established the 7-methyl cyclohexenone ring. HMBC correlations from olefinic proton H-4 to C-3/C-5/C-8a, from oxygenated methylene proton H-1 to C-3/C-4a/C-8a displayed the presence of a dihydropyran ring. The side chain C-9/C-10/C-11 was adjacent to C-3 supported by HMBC correlations from H-9 to C-3 and from H-4 to C-9. Thus, the azaphilone skeleton was established. HMBC correlations from oxygen-bearing methine proton H-8 to carbonyl carbon C-13 suggested that the orsellinic acid moiety attached to C-8 (Fig. 3). Therefore, the planar structure of **4** was determined, which was same as that of a known azaphilone analogue Sch 725680 (**10**)[19], but with different relative configuration.

The relative configuration of **4** was determined on the basis of $^{1}H-^{1}H$ coupling constants and NOESY experiments. The coupling constant of $J_{8,8a}$ = 2.8 Hz indicated the *syn* relationship of H-8/H-8a. In the NOESY spectrum, NOE correlations of H-8 with Me-12 and H-8a suggested that these protons were placed on the same side of the molecule (Fig. 4). The absolute configuration of **4** was determined by the circular dichroism (CD) exciton chirality method[34,35]. The CD spectrum of **4** showed Cotton effects involved in the conjugated trienone chromophores interacting with benzoate at 360 and 306 nm ($\Delta\varepsilon$ −1.61 and 0.57), suggesting the 8*S* configuration. Therefore, the absolute configuration of **4** was established as 7*S*, 8*S*, 8a*R* and it was named dangelone A.

Analysis of NMR data (Tables S4 and S5) of compounds **5** and **6** suggested that they had the similar azaphilone plane frame as **4** and the distinction between them lay the respective side chains at C-3. In the side chain of **5**, a hydroxymethyl group at C-11 [δ_H 4.09 (d, J = 13.6 Hz, 2H), δ_C 60.6, and δ_H 4.98 (t, J = 5.1 Hz, OH-11)] was present instead of C-11 methyl group (δ_C 18.1) in **4**. The COSY correlations of H-9/H-10/H-11/OH-11 and HMBC correlations from H-11 to C-9/C-10 confirmed the side chain assignment of **5**. In the side chain of **6**, a free C-11 carboxyl group (δ_C 166.8) replaced the C-11 methyl in **4**, which was verified by HMBC correlation from H-9 to C-11. The relative configurations of **5** and **6** were in accordance with that of **4** based on NOESY spectra. By comparing the CD spectra and optical rotation with those of **4**, the absolute configurations of **5** and **6** were both determined as 7*S*, 8*S*, 8a*R* and they were named dangelones B and C, respectively.

Compound **7** possessed the molecular formula $C_{23}H_{24}O_9$ on the basis of HRESIMS ($[M+Na]^+$, *m/z* 467.1328; Calcd. for $C_{23}H_{24}O_9Na$, 467.1313). The ^{1}H and ^{13}C NMR data (Tables S4 and S5) of **7** showed an additional acetyl group signals at δ_H

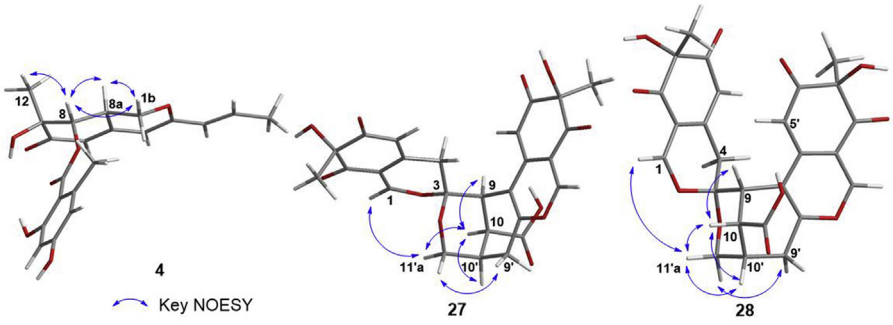

Figure 4 Key NOESY correlations of compounds **4**, **27**, and **28**.

2.02 (3H, s, H-22) and δ_C 20.7 (C-22), 170.6 (C-21) by comparison to those of pinophilin B (**11**)[20]. HMBC correlations from oxygenated methylene protons H_2-11 (δ_H 4.70) to carbonyl carbon C-21 (δ_C 170.6) and from methyl protons H_3-22 (δ_H 2.02) to C-21 confirmed that the acetyl group was attached to the terminal C-11 hydroxy in **11**. Thus, **7** was an acetylated derivative of **11** and named dangelone D.

Compound **8** was established the molecular formula $C_{21}H_{22}O_9$ by positive HRESIMS at *m/z* 419.1352 $[M+H]^+$ (Calcd. for $C_{21}H_{23}O_9$, 419.1337), two more hydrogens than that of pinazaphilone B (**12**)[21]. Comparing the ^1H and ^{13}C NMR data (Tables S4 and S5) of **8** with those of **12** indicated that a *trans*-olefin double bond (δ_C 137.5, 125.5) at C-9 (C-10) in **12** was replaced by two methylene [δ_H 2.55 (2H, overlap, H-9), 2.56 (2H, overlap, H-10) and δ_C 31.1 (C-9), 30.5 (C-10)] in **8**, suggesting that **8** was a hydrogenated derivative of **12** at C-9 and C-10, which was confirmed by HMBC correlations from methylene protons H_2-9 (δ_H 2.55) to C-3/C-4/C-10/C-11. The relative configurations of **7** and **8** were established to be same as that of **12** by the similar $J_{8,8a}$ coupling constants and NOESY spectra, respectively. Since the CD spectra of **7** and **8** agree well with those of **10**[19] and **12**[21], respectively (Supporting Information Figs. S283 and S284), the absolute configurations of **7** and **8** were both assigned as 7*S*, 8*S*, 8a*S*. Then, **8** was named dangelone E.

Comparing the NMR data (Tables S4 and S5) of compound **9** with those of **12**[21], an oxygenated methine was observed at δ_H 4.00 (d, J = 4.4 Hz, H-6) and δ_C 74.3 (C-6) in **9**, with the disappearance of ketone carbonyl carbon at δ_C 197.3 in **12**. HMBC correlations from the oxygenated methine proton H-6 to C-4a/C-5/C-7/C-12, from H-12 to C-6/C-7/C-8, and from H-5 to C-4/C-7/C-8a indicated that ketone carbonyl group at C-6 in **12** was reduced to a hydroxy in **9**. The *trans*-diaxial relationship of H-8/H-8a was deduced from the coupling constant ($J_{8,8a}$ = 10.1 Hz). The NOESY correlations between H-6/H-12/H-8 suggested that they were placed on the same side of the molecule. To determine the absolute configuration of **9**, the CD spectrum was measured in methanol and compared with its calculated electronic circular dichroism (ECD) of 6*R*,7*R*,8*S*,8a*S*-**9** and 6*S*,7*S*,8*R*,8a*R*-**9** using the quantum chemical method[36]. The predicted ECD spectrum of 6*R*,7*R*,8*S*,8a*S*-**9** exhibited an excellent fit with the experimental one (Supporting Information Fig. S285). Thus, the absolute configuration of **9** was assigned to be 6*R*, 7*R*, 8*S*, 8a*S* and it was named dangelone F.

Compound **18** was obtained as a yellow amorphous powder and had a molecular formula of $C_{26}H_{28}O_{13}$ on the base of HRESIMS $[M+Na]^+$ *m/z* 571.1429 (Calcd. for $C_{26}H_{28}O_{13}Na$, 571.1422). The ^1H and ^{13}C NMR data (Supporting Information Table S6) exhibited additional five oxygenated carbons (δ_C 101.1, 73.0, 70.7, 88.1, 62.9), an anomeric proton at δ_H 5.67 (d, J = 4.5 Hz), and six hydrogens between δ_H 3.66−4.21 by comparing their NMR data with those of 6, indicating the presence of a α-ribose[37], which was confirmed by $^1H-^1H$ COSY and HMBC correlations. The α-ribose was connected to C-17 in orsellinic acid moiety supported by HMBC correlation from anomeric proton H-1′ to C-17. The sugar moiety in **18** was determined as D-ribose by comparing the retention time in LC–MS of the thiocarbamoyl-thiazolidine derivative of the acid hydrolysate of **18** with those of authentic D-ribose and L-ribose (Supporting Information Fig. S7). Due to the same relative configuration and similar CD spectrum by comparing with those of **6**, the absolute configuration of the aglycone in **18** was established as 7*S*, 8*S*, 8a*R*, which was further confirmed by ECD calculations[36]. The calculated weighted ECD spectrum of 7*S*,8*S*,8a*R*-**18** agrees well with the experimental spectrum of **18** (Supporting Information Fig. S286). Thus, **18** was determined to be 17-*O*-α-D-ribosyl-dangelone C and named dangeloside A.

The NMR spectroscopic data (Table S6) of compound **19** closely resembled those of Sch 725680 (**10**)[19], except for the presence of an additional ribose moiety, the ^{13}C NMR data of which was in good accordance with those of α-ribose moiety in **18**. HMBC correlation from anomeric proton H-1′ to C-17 suggested that ribose was linked to C-17. Due to the limitation of the trace amount of **19**, the configuration of D-ribose in **19** was determined according to the same biosynthetic origin of suger moiety in **18**. The relative configuration of the aglycone in **19** was same as that of **10** based on NOESY spectrum. The absolute configuration of the aglycone in **19** was identified as 7*S*, 8*S*, 8a*S* by comparison of the CD spectrum with those of **10** (Supporting Information Fig. S287). Thus, **19** was determined to be 17-*O*-α-D-ribosyl-Sch 725680 and named dangeloside B.

Compound **20** was isolated as a light yellow powder, HRESIMS analysis of **20** gave an ion $[M+H]^+$ at *m/z* 777.2205 consistent with a molecular formula of $C_{43}H_{36}O_{14}$ (Calcd. for $C_{43}H_{37}O_{14}$, 777.2178). Acquisition of ^1H, ^{13}C, HSQC NMR spectra of **20** showed only 21 carbons, the presence of an orsellinic acid moiety, and signals of azaphilone skeleton, including a downfield shifted olefinic proton at δ_H 8.08 (s), two ketone carbonyl at δ_C 193.8, 193.6, a propenyl group at δ_H 5.78 (dd, J = 15.6, 1.3 Hz), 6.51 (dq, J = 15.6, 6.9 Hz), 1.67 (d, J = 6.9 Hz), δ_C 124.1, 137.0, 18.7 (Supporting Information Tables S7 and S9). These signals were very similar to those of **16**, a known compound (−)-mitorubrin[25], except for the presence of an additional methylene (δ_H 3.67, δ_C 19.6) in **20**. According to its molecular formula, **20** was presumed to be composed of two

same azaphilone monomer moieties similar to **16**. Furthermore, HMBC correlations from the additional methylene protons H_2-21 (δ_H 3.67) to C-4a/C-5/C-6, from H-1 to C-3/C-4a/C-8/C-8a, from H-4 to C-3/C-4a/C-8a/C-9, and from H-9 to C-3/C-4/C-10/C-11 confirmed that **20** was a symmetric azaphilone dimer connected by a C-21 methylene bridge to C-5 and C-5′ in two same azaphilone monomer moieties, respectively. Then, **20** was named didangelone A.

Compound **21** was isolated as yellow powder; its molecular formula was determined as $C_{43}H_{36}O_{15}$ by HRESIMS ($[M+H]^+$, *m/z* 793.2121; Calcd. for $C_{43}H_{37}O_{15}$, 793.2127), one more oxygen than that of **20**. The ^{13}C NMR data (Table S9) of **21** were closely related to those of **20** except that the signal for C-11 at δ_C 18.7 in **20** was shifted downfield to δ_C 62.9 in **21**, which indicated that **21** was the 11-hydroxy derivative of **20**. HMBC correlations from H-11 to C-9/C-10 confirmed the location of hydroxy group at C-11. Then, **21** was named didangelone B.

The molecular formula $C_{43}H_{36}O_{16}$ of compound **22** was established by HRESIMS ($[M+Na]^+$, *m/z* 831.1918; Calcd. for $C_{43}H_{36}O_{16}Na$, 831.1896). Analysis of the NMR spectra indicated that **22** also was a completely symmetrical azaphilone dimer. The NMR data (Tables S7 and S9) of **22** showed very similar signals to those of **20**. The differences were that a methyl group (δ_H 1.67, δ_C 18.7) at C-11/C-11′ in **20** was replaced by a hydroxymethyl group (δ_H 4.07, δ_C 60.6) in **22**, respectively, which was elucidated by $^1H-^1H$ COSY correlations of H-9/H-10/H-11 and HMBC correlations from hydroxymethyl proton H-11 to C-9/C-10. Then, **22** was named didangelone C.

Compound **23** was isolated as a red amorphous powder. The molecular formula of **23**, $C_{43}H_{37}NO_{13}$, was established by its HRESIMS spectrum ($[M+H]^+$, *m/z* 776.2358; Calcd. for $C_{43}H_{38}NO_{13}$, 776.2338), which showed that a nitrogen atom replaced an oxygen atom comparing with that of **20**. The ^1H and ^{13}C NMR spectra (Tables S7 and S9) showed the typical signals of methylene-bridged azaphilone dimer. Detailed analysis of its NMR spectrum revealed that comparing with C-1′ and C-3′, the resonances for C-1 and C-3 were shifted up-field by 15.6 and 11.3 ppm, respectively, which suggested that an oxygen atom from one of pyran ring in **20** was replaced by a nitrogen atom to become a pyridine ring. Then, **23** was named didangelone D.

Compound **24** was also a red amorphous powder, its molecular formula was determined as $C_{43}H_{37}NO_{15}$ by HRESIMS ($[M+H]^+$, *m/z* 808.2291; Calcd. for $C_{43}H_{38}NO_{15}$, 808.2295). The NMR data (Tables S7 and S9) of **24** were similar to those of **23**, indicating that **24** was also a nitrogenous azaphilone dimer with a pyridine ring. The differences from **23** were that two methyl group (δ_H 1.51 and 1.55, δ_C 18.74 and 18.65) at C-11 and C-11′ in **23** was replaced by two hydroxymethyl group (δ_H 3.85 and 3.81, δ_C 60.7 and 60.9) in **24**, respectively, which was confirmed by HMBC correlations from H-11 (δ_H 3.85) to C-9/C-10 and from H-11′ (δ_H 3.81) to C-9′/C-10′. Then, **24** was named didangelone E.

The absolute configuration of **20** was determined by ECD calculations[36]. It was found that the calculated weighted ECD spectra of 7*R*,7′*R*-**20** were in good accordance with the experimental CD spectra of **20** (Supporting Information Fig. S288). Consequently, the absolute configuration of **20** was identified as 7*R*, 7′*R*. Likewise, the CD curve similarities between **21**, **22**, **23**, **24** and **20** indicated that they bear the same configurations.

Compound **25** was isolated as a light yellow amorphous powder. Its molecular formula $C_{42}H_{34}O_{17}$ was established by HRESIMS ($[M+H]^+$, *m/z* 811.1860; Calcd. for $C_{42}H_{35}O_{17}$, 811.1869). The 1D NMR (Supporting Information Tables S8 and S9) and HSQC data showed four ketone carbonyl carbons C-6/C-8/C-6′/C-8′ (δ_C 194.8/194.0/195.0/193.9), two oxygenated quaternary carbon C-7/C-7′ (δ_C 86.6/86.2), two downfield shifted olefin protons H-1/H-1′ (δ_H 8.15/8.23), and two orsellinic acid moieties. Based on these features, the NMR data of **25** were closely related to those of a known azaphilone dimer diazaphilonic acid (**26**)[27,28] except that the carboxyl group at C-11 (δ_C 174.7) in **26** was replaced by a hydroxymethyl group [δ_H 3.65 (d, J = 7.2 Hz, 2H), δ_C 63.7] in **25**, which was confirmed by HMBC correlations from H-11 (δ_H 3.65) to C-9/C-10 and $^1H-^1H$ COSY correlations of H-11/H-10(H-10′)/H-9. Thus, the planar structure of **25** was determined. The relative configuration of **25** was established on the basis of NOESY experiment. The NOE correlations of H-11 with H-9/H-10′/H-9′a suggested that these protons were placed on the same side of the molecule. According to its biosynthesis pathway same as that of azaphilone monomer, the absolute configuration of C-7 and C-7′ was assigned as *R*. ECD calculations were conducted to clarify the absolute configuration of **25**[36]. The calculated weighted ECD spectra of 9*R*,10*R*,10′*R*,7*R*,7′*R*-**25** and 9*S*,10*S*,10′*S*,7*R*,7′*R*-**25** have obvious differences, revealing that the calculated ECD spectrum of 9*R*,10*R*,10′*R*,7*R*,7′*R*-**25** agrees well with the experimental one (Supporting Information Fig. S289). Therefore, the absolute configuration of **25** was assigned as 9*R*, 10*R*, 10′*R*, 7*R*, 7′*R* and it was named didangelone H.

Compound **27** was isolated as a light yellow amorphous powder. HRESIMS spectrum established its molecular formula as $C_{42}H_{34}O_{17}$ ($[M+H]^+$, *m/z* 811.1829; Calcd. for $C_{42}H_{35}O_{17}$, 811.1869), showing 26 degrees of unsaturation. 1D NMR (Tables S8 and S9) and HSQC spectra displayed typical signals for azaphilone dimer, including four ketone carbonyl carbons C-6/C-8/C-6′/C-8′ (δ_C 195.4/193.4/194.7/194.3), two downfield shifted olefin protons H-1/H-1′ (δ_H 7.90/8.13), and two orsellinic acid moieties. The ^{13}C NMR data and HMBC interactions from H-1 to C-3/C-4a/C-8/C-8a and from H-1′ to C-3′/C-4a′/C-8′/C-8a′ established two orsellinic acyl substituted azaphilone pyranoquinone bicyclic cores similar to that of **16**. In one of azaphilone cores, a double bond at C-3 and C-4 was reduced, which was supported by HMBC correlations of H-1 to C-3 (δ_C 104.3) and of H_2-4 (δ_H 3.19/2.82) to C-3/C-4a/C-5/C-8a. In addition to above mentioned two orsellinic acyl substituted azaphilone cores, the remaining ^{13}C NMR data showed only one unsaturated carboxyl carbon signal at δ_C 176.3 (C-11), indicating two unassigned degrees of unsaturation. Therefore, **27** was presumed to be dimerized though two rings by two orsellinic acyl substituted azaphilone bicyclic cores. $^1H-^1H$ COSY cross-peaks of H-9/H-10/H-10′(H-9′)/H-11′ and HMBC interactions from methine proton H-9 to C-3, and from oxygenated methylene protons H-11′ to C-3/C-9′ established a tetrahydropyran ring connecting with a dihydropyran ring of azaphilone core though spiral carbon C-3 (Fig. 3). HMBC correlations from H-9 to C-3′/C-4′/C-4a′, and from methylene proton H-9′ to C-3′/C-10′/C-11′ indicated a cyclohexene ring fused with a pyran ring of another azaphilone core though double bond at C-3′(C-4′), then establishing the polycyclic bridged heterocycle and spiral structures, tetrahydro-3-oxaspiro [bicyclo [3.3.1]nonane-2,2′-pyran] core. HMBC correlation from H-10 to C-11 suggested a carboxyl group attached to C-10. Thus, the planar structure of **27** was established. The signals for two active conjugated olefin protons H-5 and H-5′ did not show in the ^1H NMR spectrum due to deuterium exchange in CD_3OD.

The relative configuration of **27** was assigned by NOESY experiment. NOESY correlations of axial H-11′a with H-1/H-10 and of H-10 with H-9/H-10′/H-11′a indicated that these protons were in the same side of the tetrahydropyran ring, whereas that of H-9′a with H-11′b suggested the other side orientation (Fig. 4). According to the same biosynthetic pathway for azaphilone monomer, the absolute configuration of C-7 and C-7′ was both assigned as *R*. ECD calculations were performed to clarify the absolute configuration of **27**[38]. The calculated weighted ECD spectra of 3*R*,9*R*,10*S*,10′*R*,7*R*,7′*R*-**27** and 3*S*,9*S*,10*R*,10′*S*,7*R*,7′*R*-**27** have obvious differences from 210 to 300 nm, revealing that the calculated ECD spectrum of 3*R*,9*R*,10*S*,10′*R*,7*R*,7′*R*-**27** agrees well with the experimental one of **27** (Supporting Information Fig. S290). Therefore, the absolute configuration of **27** was determined as 3*R*, 9*R*, 10*S*, 10′*R*, 7*R*, 7′*R* and it was named didangelone F.

Compound **28** possessed the molecular formula $C_{42}H_{34}O_{17}$ deduced from its HRESIMS ($[M+Na]^+$, *m/z* 833.1708; Calcd. for $C_{42}H_{35}O_{17}Na$, 833.1688) and ^{13}C NMR. The planar structure of **28** was found to be same as that of **27** by detailed interpretation of its 1D and 2D NMR data (Tables S8 and S9). **28** differs from **27** only in the stereochemistry at C-3/C-9/C-10/C-10′, of which the relative configuration for C-3/C-9/C-10/C-10′ was same as that of **27** according to analysis of NOESY spectrum (Fig. 4). Using the same computational methods as that of **27**, the absolute configuration of **28** was finally determined as 3*S*, 9*S*, 10*R*, 10′*S*, 7*R*, 7′*R* based on its CD curve similarities with ECD spectra of 3*S*,9*S*,10*R*,10′*S*,7*R*,7′*R*-**28** (Supporting Information Fig. S290)[38], which is actually a diastereoisomer of **27** and it was named didangelone G.

Compound **29** was isolated as a yellow amorphous powder. Its molecular formula was identified as $C_{64}H_{52}O_{24}$ according to HRESIMS ($[M+H]^+$, *m/z* 1205.2882; Calcd. for $C_{64}H_{53}O_{24}$, 1205.2921). 1D NMR (Supporting Information Tables S10 and S11) and HSQC data showed three sets of typical azaphilone monomer signals, including six ketone carbonyl carbons, three oxygenated olefin protons, and three orsellinic acid moieties, indicating that **29** was probably an azaphilone trimer. A detailed comparison of ^1H and ^{13}C NMR data between **29**, **27** and **20** disclosed that except for the presence of an azaphilone dimer moiety similar to **27**, an additional methylene (δ_H 3.25/3.12, δ_C 20.9) and an orsellinic acyl substituted azaphilone monomer moiety, resemble to the half fragment of **20**, were present in **29**. HMBC correlations from the additional methylene protons H_2-21 (δ_H 3.25/3.12) to C-5/C-6/C-4a″/C-5″ revealed that a C-21 methylene bridge connected C-5″ in an azaphilone monomer to C-5 in an azaphilone dimer moiety similar to **27**. Thus, the planar structure of **29** was established. According to NOESY correlations, the relative configuration for C-3/C-9/C-10/C-10′ of **29** was same as that of **27**. As the CD spectra of **29** with **27** highly coincidence, the absolute configurations of **29** was assigned as 3*R*, 9*R*, 10*S*, 10′*R*, 7*R*, 7′*R*, 7″*R*. Then, **29** was named tridangelone A.

Compound **30** has the same molecular formula as **29**, $C_{64}H_{52}O_{24}$, deduced from HRESIMS ($[M+Na]^+$, *m/z* 1227.2653; Calcd. for $C_{64}H_{52}O_{24}Na$, 1227.2682). Interpretation of 1D and 2D NMR data (Tables S10 and S11) disclose that **30** and **29** possess the same planar structure. **30** differs from **29** only in the stereochemistry at C-3/C-9/C-10/C-10′. According to NOESY correlations, the relative configuration for C-3/C-9/C-10/C-10′ of **30** was same as that of **28**. The CD curve similarities between **30** and **28** indicated that the absolute configuration of **30** was established as 3*S*, 9*S*, 10*R*, 10′*S*, 7*R*, 7′*R*, 7″*R*, which is actually a diastereoisomer of **29** and it was named tridangelone B.

Compounds **31** and **32** were assigned to have the same planar structure by analysis of their HRESIMS and NMR data. Comparison of the ^1H and ^{13}C NMR data (Tables S10 and S11) between **31** and **29** suggested that **31** was a 11″-hydroxy derivative of **29**, which was supported by HMBC correlations from hydroxymethyl proton H-11″ (δ_H 4.14) to C-9″/C-10″. According to NOESY correlations, the relative configurations for C-3/C-9/C-10/C-10′ of **31** and **32** were same as those of **29** and **30**, respectively. The absolute configurations of **31** and **32** were respectively determined as 3*R*, 9*R*, 10*S*, 10′*R*, 7*R*, 7′*R*, 7″*R* and 3*S*, 9*S*, 10*R*, 10′*S*, 7*R*, 7′*R*, 7″*R* by comparing their CD spectra with those of **29** and **30**. Then, **31** and **32** were named tridangelones C and D, respectively.

Compound **33** was isolated as a yellow amorphous powder. The molecular formula of **33** was determined to be $C_{64}H_{54}O_{24}$ on the basis of HRESIMS data ($[M+Na]^+$, *m/z* 1229.2950, Calcd. for $C_{64}H_{54}O_{24}Na$, 1229.2897), one fewer oxygen and two more hydrogens than **31**. The ^1H and ^{13}C NMR spectra (Tables S10 and S11) of **33** and **31** showed very similar signals, with the exception that the carboxyl carbon signal at δ_C 172.6 (C-11) in **31** was replaced by the signals assigned to hydroxymethyl group at δ_H 3.27/3.19 and δ_C 60.9 in **33**. These data indicated that the carboxyl group at C-11 in **31** was substituted by a hydroxymethyl group in **33**, which was supported by $^1H-^1H$ COSY correlation of H-11/H-10 and HMBC correlation from H-11 to C-9/C-10. According to NOESY correlations, the relative configuration for C-3/C-9/C-10/C-10′ of **33** was same as that of **31**. Likewise, the CD curve similarities between **33** and **31** suggest that they bear the same absolute configurations and **33** was named tridangelone E.

Compound **34** was obtained as a yellow powder. HRESIMS analysis gave an $[M+Na]^+$ ion at 585.1382 (Calcd. for $C_{30}H_{26}O_{11}Na$, 585.1367), consistent with a molecular formula of $C_{30}H_{26}O_{11}$. Comparison of the NMR data (Supporting Information Table S12) of **34** with those of (−)-mitorubrin (**16**)[25] indicated the presence of three fragments, an orsellinic acyl substituted azaphilone monomer moiety similar to **16** (fragment A), an additional methylene (δ_H 3.40/3.76, δ_C 17.8), and a 3-substituted 2,4-dihydroxy-6-methylbenzoic acid moiety (fragment B). HMBC correlations from the methylene protons H-21 (δ_H 3.40/3.76) to C-5/C-4a/C-6/C-22/C-23/C-27 suggested that the methylene bridge at C-21 respectively linked to C-5 in fragment A and C-22 in fragment B. Thus, the planar structure of **34** was established. The absolute configuration of **34** was determined as 7*R* by comparing its CD spectra with those of (−)-mitorubrin (**16**)[25,39] and it was named dangelone G.

Compound **35** was obtained as a yellow amorphous powder. Its molecular formula of $C_{20}H_{18}O_6$ was determined on the basis of HRESIMS ($[M-H]^-$, *m/z* 353.1032; Calcd. for $C_{20}H_{17}O_6$, 353.1030). The ^1H, ^{13}C, and HSQC NMR (Table S12) spectra showed the presence of an aldehyde group at δ_H 9.81(s), δ_C 195.0, two methyl groups at δ_H 1.86/2.00 and δ_C 21.2/7.2, six aromatic protons at δ_H 6.07/6.11/6.21/5.89/6.34/7.46, and a methine at δ_H 6.42 and δ_C 39.3. HMBC correlations (Fig. 3) from methyl proton H-13 (δ_H 2.00) to C-9/C-10/C-11, from aldehyde proton H-14 (δ_H 9.81) to C-8/C-9, and from aromatic proton H-12 (δ_H 6.07) to C-7/C-8/C-10/C-11 established a 6-substituted 2,4-dihydroxy-3-methylbenzaldehyde (fragment C). $^1H-^1H$ COSY correlations of H-4/H-5/H-6 and HMBC correlations from H-4 to C-2/C-6 and from H-6 to C-2/C-4/C-5 confirmed a 2-substituted furan ring (fragment D). Additionally, the ^1H NMR spectrum showed the

presence of two *meta*-position protons of benzene ring at δ_H 6.21 (d, J = 2.3 Hz, H-17), 6.11 (d, J = 2.3 Hz, H-19). HMBC correlations from methyl protons H-21 (δ_H 1.86) to C-15/C-19/C-20, from H-17 to C-15/C-18/C-19, and from H-19 to C-15/C-17/C-18 established a 4-substituted 1,3-dihydroxy-5-methylbenzene (fragment E). The key HMBC correlations from methine proton H-1 (δ_H 6.42) to C-2/C-6/C-7/C-8/C-12/C-15/C-16/C-20 indicated that the C-1 methine bridge connected to C-7 in fragment C, C-2 in fragment D, and C-15 in fragments E, respectively (Fig. 3). Thus, the planar structure of **35** was established. Finally, ECD computational methods were used to clarify the absolute configuration of **35**. The conformers of 1*R*-**35** and 1*S*-**35** were calculated by using the Gaussian 09[36] software (Revision C.01, Gaussian Inc., Wallingford, CT, USA, 2010). It was found that the calculated weighted ECD spectra of 1*R*-**35** are in good accordance with the experimental CD spectrum of **35** (Supporting Information Fig. S291). Consequently, the 1*R* configuration of **35** was assigned and it was named dangelone H.

2.4. Bioactivities evaluation

Cytotoxic activities of all isolated compounds were evaluated against two human cancer lines HepG-2 and MCF-7 in the MTT assay. Taxol was used as a positive control, with IC_{50} values of 1.28 (HepG2) and 2.31 (MCF-7) μmol/L, respectively. Compounds **14**, **5**, **10**, and **11** exhibited cytotoxicities against HepG2 cells with IC_{50} values of 2.83, 6.82, 7.78, and 11.4 μmol/L, respectively. Compounds **14**, **10**, and **5** showed potent inhibition against MCF-7 cells with IC_{50} values of 5.53, 14.63, and 14.98 μmol/L, respectively, while the other compounds were inactive (IC_{50} > 20 μmol/L, Supporting Information Table S13). Comparing the structure of compounds **14**, **5**, and **11** with that of the other azaphilone monomers, orsellinic acid esterification at C-8 (**14** *vs*. **17**), double bond between C-8a and C-1 (**14** *vs*. **5** and **11**), and hydroxy at C-11 (**14**, **5**, **11** *vs*. the others) significantly increase the activity, indicating the important contribution effects on cytotoxicity.

In addition, compounds **4**–**39** were also assessed for their anti-inflammatory and antioxidant inhibitory activities, with curcumin as a positive control (inhibitory rates 93.7 ± 2.5% at 10^{-5} mol/L and 91.2 ± 3.2% at 10^{-4} mol/L, respectively). At a concentration of 10^{-5} mol/L, compound **13** was found to be significant inhibitory effect on NO production induced by lipopolysaccharide (LPS) in murine microglial BV2 cell with inhibitory rate of 96.0 ± 4.6% (Supporting Information Table S14). Four compounds **21**, **31**, **34**, and **36** were found to possess potent antioxidant activities against lipid peroxidation induced by Fe^{2+}-cystine in rat liver microsomal with inhibitory rates of 68.7 ± 4.2%, 64.8 ± 2.6%, 66.7 ± 4.5%, and 63.5 ± 5.2%, respectively, at a concentration of 10^{-4} mol/L (Supporting Information Table S15). Interestingly, although the azaphilone monomers **16** and **17** showed no antioxidant activities and cytotoxicities, the azaphilone dimer **21** and trimer **31** exhibited potent antioxidant activities.

The antioxidant activities of compounds **4**–**39** were evaluated by measuring the inhibitory rates of malondialdehyde (MDA) in rat liver microsomal lipid peroxidation induced by Fe^{2+}-cystine *in vitro* according to the reported anti-inflammatory activities of compounds **4**–**39** were assessed by measuring the inhibitory effects on NO production induced by lipopolysaccharide (LPS) in murine microglial BV2 cell line according to the reported procedures.

2.5. Characterization of the gene cluster for azaphilones biosynthesis

To understand the biosynthesis of these azaphilones, we analyzed the PKSs in the genome of *P. dangeardii*. BLAST search against the non-reducing PKS (NR-PKS) AzaA in the *aza* cluster[40] and MrpigA in the *MonAzPs* cluster[41], which were responsible for the biosynthesis of azanigerones and *Monascus* azaphilone pigments (MonAzPs), respectively, revealed two NR-PKSs (DanE and DanE′) with high protein identities (>55%) on Contig 60. A detailed bioinformatic analysis of adjacent genes of these two NR-PKSs identified two attractive neighbouring dual PKSs gene clusters, which were designated as *dan1* and *dan2* (Supporting Information Fig. S292A). Since multiple PKS genes located in a same gene cluster are common for fungal genomes[42] and it has been reported that two or three PKSs synthesize a polyketide product either organized in sequence[43,44] or in convergence[45], the combination of *dan1* and *dan2* clusters responsible for the biosynthesis of isolated azaphilones is reasonable. In the *dan1* and *dan2* clusters, the predicted domains of NR-PKSs DanE and DanE′ were same as starter unit: ACP transacylase (SAT), ketosynthase (KS), acyltransferase (AT), product template (PT), C-methyltransferase (MT), acyl carrier protein (ACP) and reductase (R; Supporting Information Tables S16 and S17). Another NR-PKS (DanV) with SAT-KS-AT-PT-ACP-ACP domains in the *dan2* cluster was proposed to involve in the formation of orsellinic acid. However, the fatty acid synthase DanG with α/β subunits in the *dan1* cluster was supposed to inactive since the absence of ACPS domain. Most of the genes in the *dan1* and *dan2* clusters have one or more corresponding homolog in the *aza* gene cluster[40] (Table S16). However, no key AzaH-like flavin-dependent monooxygenase, which is involved in C-7 hydroxylation and pyran-ring formation to afford the characteristic pyrano-quinone bicyclic core in azaphilones[40], was presented in the *dan2* cluster. These features suggest that the pair of gene clusters might redundantly or collaboratively biosynthesize the novel azaphilone derivatives with structure diversity.

To verify the gene clusters responsible for azaphilones biosynthesis, a pathway specific transcriptional factor *danS* was overexpressed through a *gpdA* gene as a strong promoter based on the homologous recombination method. The metabolites from the overexpressed mutant *gpdA::danS* were extracted and analyzed by LC–MS (Supporting Information Fig. S4). Comparing to the metabolites from wild type *P. dangeardii* which did not produce any azaphilones, various azaphilones were detected in the mutant *gpdA::danS*, suggested that the *dan* gene clusters were responsible for azaphilones biosynthesis.

2.6. Proposed biosynthetic pathway for azaphilones from the dan1 and dan2 clusters

A putative biosynthetic pathway of azaphilones was proposed (Supporting Information Fig. S292B). Started from the NR-PKS DanE or DanE′ assembling the hexaketide precursor, an aldehyde intermediate was released. Then, the terminal ketone is reduced to alcohol **i** by the ketoreductase DanU (61% identity to AzaE). The FAD-dependent monooxygenase DanB, a homology of AzaH (59% identity) which is the only enzyme responsible for benzaldehyde hydroxylation and the formation of pyran ring during azanigerone biosynthesis[40], is proposed to catalyze the hydroxylation of C-7 in **i**, which triggers the pyran ring formation to yield **ii**. Then, *O*-acetyltransferase DanN/DanN′ catalyzes the

acetylation of **ii** at 10-OH, followed by the acetic acid elimination catalyzed by the dehydratase DanW to afford **iii**. In parallel, NR-PKS DanV is responsible for the generation of orsellinic acyl chain and *O*-acetyltransferase DanC/DanC′ directly transferred the orsellinic acyl-ACP to the C-7 hydroxy of **iii**. Previous studies demonstrated that cytochrome P450 oxygenases are able to catalyze the terminal methyl into alcohol, aldehyde, or acid through one to three consecutive oxidation steps, examples including P450-1 and P450-4 for gibberellin biosynthesis, CYP71AV1 for artemisinic acid biosynthesis, and AsCYP51H10 for the biosynthesis of antimicrobial triterpenes[46]. The terminal C-11 methyl in **16**, **13**, **4**, and **10** could be hydroxylated by cytochrome P450 DanM to afford **17**, **14**, **5**, and **11**, respectively, and further oxidized to yield **15**, **6**, and **12** catalyzed by DanM.

For the biosynthesis of azaphilone polymers, we hypothesize that the C-5(4a) double bond of the azaphilone monomer **I** is reduced by aldoketoreductase DanK (Fig. S292B), an orthologue of NAD(P)H-dependent oxidoreductase MrPigE[41] (69% identity), to yield intermediate **II**. The aldolase DanY is proposed to catalyze the enolization of C-6 ketone in **II** and introduce a hydroxymethyl at C-5 from formaldehyde, followed by dehydration to generate the reactive enone intermediate **III**. The enzyme with similar function has been reported, such as the α-methylserine aldolase from *Variovorax paradoxus*, which is responsible for conversion from L-alanine to α-methyl-L-serine accompanied by hydroxymethyl transfer from formaldehyde[47]. Michael addition between **I** and **III** yields the methylene-bridged azaphilone dimers (**20**−**24**). While non-enzymatic intermolecular Diels−Alder cycloaddition between two molecular of **I** results in the production of azaphilone dimers. Finally, azaphilone trimers (**29**−**33**) could be generated from combination of Michael addition and Diels−Alder cycloaddition between different azaphilone dimers with a third azaphilone monomer.

2.7. *Discussion*

Due to the potential of endophytic fungi to produce structurally diverse and biologically active secondary metabolites, various strategies for inducing the expression of silent biosynthetic gene clusters (BGCs) have been developed. However, no any strategies could be universal for all strains. The metabolic shunting strategy applied here is basically adapted from "Robin Hood" who robbed the wealthy to relieve the indigent. Inhibiting the biosynthesis of main metabolites in wild type strain would save the common building blocks (such as acetyl-CoA and malonyl-CoA for PKSs) to be readily competitively acquired by other BGCs, and induce the expression of cryptic gene clusters responsible for the biosynthesis of natural products required the saved building blocks. Results from RT-PCR (Fig. S3) also supported the up-regulated expression of four additional genes encoding PKS in the mutant strain. Since polyketide precursors such as acetyl-CoA and malonyl-CoA were reserved by elimination of rubratoxins biosynthesis, three genes encoding PKS in contig 60 responsible for azaphilones biosynthesis were activated and showed high expression, which consequently led to the predominant azaphilones production in the mutant strain. In addition, trace metabolites could become detectable without the presence of main metabolites. Consequently, a siderophore peptide desferritriacetylfusigen (**39**) was found only from the mutant strain *ΔrbtJ* although the gene encoding NRPS in contig 23 was expressed in both wild type and mutant strain.

Previously, an approach of genetic dereplication has been reported[48−50] to discover novel natural products (especially trace metabolites) from fungi, which eliminated the production of major metabolites and made minor compounds detectable. Our strategy based on metabolic shunting and OSMAC is different in principle from genetic dereplication, and leads to the activation of cryptic gene clusters, besides letting trace metabolites detectable. The combinational application of metabolic shunting and OSMAC strategy is helpful to predict the biosynthesis and accumulation of specific types of natural products according to the deleted core gene type.

Although azaphilone monomers have been isolated from many other *Penicillium* strains[21], such as *Penicillium commune*[51] and *Penicillium pinophilum*[20,52], inducing the expression of silent BGCs in *P. dangeardii* led to the production of many structurally complex azaphilone dimers and trimers with methylene and polycyclic bridged heterocycle and spiral structures.

Therefore, our established combinational strategy based on metabolic shunting and OSMAC is efficient and readily handled, and would be a perfect complement to other approaches of globally activating silent BGCs. This strategy has large potential to be applied for genome mining of other fungi or bacteria for discovering numerous novel secondary metabolites with a range of attractive bioactivities.

3. Conclusions

An approach combined metabolic shunting and OSMAC strategy was applied to successfully activate cryptic BGCs in the endophytic fungus *P. dangeardii*, which led to the production of numerous new compounds with diverse structure and biological activities. Remarkably, a group of unprecedented methylene-bridged and polycyclic azaphilone dimers and trimers were found for the first time. The biosynthetic gene cluster of these azaphilones was identified through overexpression of a pathway transcription factor in azaphilones cluster. Bioinformatic analysis of the interesting pair of *dan1* and *dan2* gene clusters helps to uncover some intriguing aspects of azaphilones biosynthetic pathway. Consequently, our work successfully develops a new strategy to rapidly and globally activate cryptic gene clusters and discover the amazing novel bioactive natural products in endophytic fungi.

4. Experimental

4.1. *Strains and cultivation conditions*

The endophytic fungus *P. dangeardii* was grown on PDA (BD Difco, Sparks, NV, USA) plate at 28 °C for 6 days for sporulation. *P. dangeardii* wild type and its mutant strains (*ΔrbtJ* and *gpdA::danS*) were stationarily cultured in PDA, PDB (BD Difco), CY (0.01% (*v*/*v*) Czapek concentrate, 0.5% yeast extract, 3% sucrose, 0.1% K_2HPO_4), YG (0.5% yeast extract, 2% glucose, 0.04% (*v*/*v*) trace element), YMEG (0.4% yeast extract, 1% malt extract, 0.4% glucose, 0.2% $CaCO_3$) and rice at 28 °C for 6 days for production of secondary metabolites. *Escherichia coli* XL1-Blue was used for standard gene cloning. *Saccharomyces cerevisiae* YEH02 was used for yeast homologous recombination *in vitro*.

4.2. Gene knockout in *P. dangeardii*

The deletion of the target gene *rbtJ* (PKS) in *P. dangeardii* was carried out by homologous recombination using the *S. cerevisiae* YEH02. The genomic DNA of *P. dangeardii* was prepared using the plant genomic DNA extraction kit (Tiangen, Beijing, China). Primers for gene knockout were listed in Supporting Information Table S18. Pairs of primers, KC78uFor/KC78uRev, KC78dFor/KC78dRev and hphFor/hphRev were used for amplification of the upstream (2.5 kb) and downstream (2.5 kb) homologous regions of *rbtJ* and *hph* (hygromycin resistance). These PCR products were ligated into linearized vector backbone derived from plasmid pRS423, introduced to YEH02 using PEG/LiAc mediated transformation, and selected on uracildropout semisynthetic media, then constructed the deletion cassette. The plasmid in the correct transformant screened by colony PCR was rescued using Zymoprep Yeast Plasmid Miniprep Kit (Zymo Research, Orange County, CA, USA) and transferred to *E. coli* for gene cloning. The correct plasmids were used as template to amplify the knockout cassette. The PCR products of knockout cassette were recovered by gel recycling kit (Axygen, Union, CA, USA) and dissolved in STC buffer (1.2 mol/L sorbitol, 10 mmol/L calcium chloride and 10 mmol/L Tris-HCl, pH 7.5).

P. dangeardii spores were induced to young germ tubes in 50 mL PDB with 1% yeast extract at 28 °C for 17 h with 180 rpm agitation (Zhicheng ZWY-103 B, Shanghai, China). Cells were collected by centrifuging at 4 °C (5000 rpm) for 5 min (Sigma 3-18 K, Gettingen, Germany), washed twice with osmotic buffer (1.2 mol/L $MgCl_2$, 10 mmol/L sodium phosphate, pH 5.8), and resuspended in the 12 mL enzyme cocktail solution (36 mg lysing enzyme and 24 mg yatalase in 1.2 mol/L $MgSO_4$, 10 mmol/L sodium phosphate buffer) in 150 mL flask at 30 °C for 6 h with 80 rpm (Zhicheng ZWY-103B). After the digestion, the enzyme solution was transferred to a new tube and an equal volume of trapping buffer (0.6 mol/L sorbitol, 10 mmol/L Tris-HCl, pH 7.0) was added before centrifuging at 4 °C (5500 rpm, Sigma 3-18 K) for 10 min. The protoplast layer was collected and washed twice with two volumes of STC buffer and centrifuged (5000 rpm, Sigma 3-18 K) for 5 min at 4 °C. Protoplast precipitated in the lower layer suspension with 100 μL STC buffer and gently mixed with 10 μg of knockout cassette DNA fragment and incubated for 1 h on the ice. 1.2 mL of PEG 4000 solution (60% PEG 4000, 50 mmol/L $CaC1_2$, 50 mmol/L Tris-HCl, pH 7.5) was added to reaction mixture, incubated at 28 °C for 20 min and plated on the regeneration selection medium (PDA, 1.2 mol/L sorbitol, 800 mg/L hygromycin B). After culturing at 28 °C for 4−5 days, the transformants were stationarily inoculated on PDB for 3 days and then extracted the genomic DNA and confirming the genotype by PCR.

4.3. RNA preparation of *P. dangeardii* and reverse transcription-PCR (RT-PCR)

P. dangeardii wild type and the *ΔrbtJ* mutant were grown on rice at 25 °C for 6 days. The mycelia were collected and used for RNA extraction by TRIZOL® Reagent (Invitrogen, Carlsbad, CA, USA). Residual genomic DNA in the extracts was digested by DNase I (2 U/μL, NEB) at 37 °C for 45 min. The cDNA was synthesized using the Transcriptor First Strand cDNA Synthesis Kit (Roche, Mannheim, Germany) with Oligo-dT primers following directions from the user manual. PCR was performed with 2 × Hieff® PCR Master Mix (YEASEN, Shanghai, China) with cDNA. Primers for RT-PCR were listed in Supporting Information Table S19.

4.4. Overexpression of transcription factor *danS* in *P. dangeardii*

The overexpression cassette was constructed in plasmid pRS423 including a *gpdA* gene which as a strong promoter replaced the native promoter in transcription factor *danS*, an upstream (2.5 kb) and a downstream (2.5 kb) homologous regions of the native promoter, and a selection marker *hph*. The genes of *gpdA* and *hph*, upstream and downstream homologous regions were amplified with the primers of OETF52uFor/OETF52uRev, hphFor/hphRev, gpdaFor/gpdaRev and OETF52dFor/OETF52dRev. Primers for overexpression of transcription factor *danS* were listed in Supporting Information Table S20. The yeast recombinant *in vitro*, preparation of the protoplasts and transformation and screening were performed as above described in gene knockout.

4.5. General experimental procedures

Optical rotations were measured in MeOH using a JASCO P-2000 spectropolarimeter (Tokyo, Japan). IR spectra were recorded using a Thermo Nicolet 5700 FT-IR spectrophotometer (Waltham, MA, USA). UV spectra were determined with JASCO V-650 instrument. High-resolution electrospray ionization mass spectra (HRESIMS) were carried out using an Agilent Technologies 6520 Accurate Mass Q-TOF LC/MS spectrometer (Santa Clara, CA, USA). The CD spectra were obtained on a JASCO J-815 spectrometer. Medium pressure liquid chromatography (MPLC) was performed using ISCO-CombiFlash®Rf 200 (Teledyne Isco, Lincoln, NE, USA) with different types C18 column. Semi-preparative HPLC was carried out on a SSI instrument (Scientific Systems Inc., Philadelphia, PA, USA) with a Series 1500 PDA detector and using a YMC-Pack ODS-A column (YMC, 5 μm, 250 mm × 10 mm) or a phenyl-hexyl column (phenomenex, 5 μm, 250 mm × 10 mm). Column chromatography (CC) was performed using middle chromatogram isolated (MCI) gel CHP 20P/P120 (Mistubishi Chemical Co., Tokyo, Japan) and Sephadex LH-20 (GE Healthcare Bio-Sciences AB, Uppsala, Sweden). Thin layer chromatography (TLC) was performed on GF254 (Qingdao Marine Chemical Factory, Qingdao, China). All LC–MS analyses were carried out on a Waters ACQUITY H-Class UPLC–MS (Milford, MA, USA) with QDA mass detector (ACQUITY UPLC® BEH, 1.7 μm, 50 mm × 2.1 mm, C18 column) using positive and negative mode electrospray ionization with a linear gradient of 5%−99% MeCN/H_2O (*v*/*v*, 0.02% formic acid) in 8 min followed by 99% MeCN/H_2O (*v*/*v*, 0.02% formic acid) for 4 min with a flow rate of 0.4 mL/min 1D and 2D NMR spectra were determined with Bruker AVIII-600 spectrometer (Rheinstetten, Germany) with a 5 mm dual cryoprobe or a Bruker AVIII-500 spectrometer or Bruker AVANCE III 800 MHz with a 5 mm broadband probe. All solvents and chemicals used in this study are of analytical grade (for extraction) or LC–MS grade (for LC–MS analysis).

4.6. Analysis, extract, and isolation of metabolites

For metabolites analysis, spores of wild type and mutant strains were inoculated in different culture media and stationarily cultured for 7 days at 28 °C. The mycelia and medium were extracted with ethyl acetate (EtOAc) and analyzed by UPLC–MS.

The strain was incubated on PDA at 28 °C for 6 days to afford spores and the spores were inoculated into the PDB at 28 °C for 4 days with 180 rpm (Zhicheng ZWY-103 B) shake to prepare the seed culture. 5 mL seed culture was inoculated into 130 Erlenmeyer flasks (500 mL), previously sterilized by autoclaving, each containing 100 g rice and 100 mL distilled water. All flasks were incubated at 28 °C for 30 days. The culture was extracted three times with EtOAc at room temperature and the EtOAc was removed under reduced pressure to yield a crude extract. The crude extract was dissolved with petroleum ether (PE) to remove the fatty oil (27 g) and the residue which is insolvable in PE was evaporated to dryness and separated by MCI CC with a gradient of H_2O, 30%, 70% and 100% MeOH, acetone to obtain five fractions (Frs. A−E).

Fr. B (5 g) was further separated with MCI CC eluted with a gradient of 10%, 20%, 50% and 100% MeOH to obtain four fractions (B1−B4). Fr. B4 (1.1 g) was applied to a Sephadex LH-20 CC eluted with MeOH to obtain 10 fractions (Frs. B4a−j), based on TLC analysis.

Fr. B4e was purified by semi-preparative HPLC on phenyl-hexyl column eluted with 29% MeCN/H_2O (*v*/*v*, 0.02% formic acid) at a flow rate of 2.0 mL/min to yield **6** (5.0 mg, t_R = 42.0 min), **8** (2.5 mg, t_R = 50.0 min), **9** (2.4 mg, t_R = 26.0 min) and **15** (4.0 mg, t_R = 34.0 min).

Fr. B4f was purified by semi-preparative HPLC on phenyl-hexyl column eluted with 34% MeCN/H_2O (*v*/*v*, 0.02% formic acid) at a flow rate of 2.0 mL/min to afford **18** (5.0 mg, t_R = 23.0 min).

Fr. C (12 g) was divided into two parts and separated by MPLC eluted with a linear gradient of 5%−95% MeOH/H_2O (*v*/*v*, 0.02% formic acid) in 130 min and 100% MeOH for 30 min at a flow rate of 50 mL/min on C18 column (SepaFlash C18, 20−45 μm, SW330, Changzhou, China) to give twenty fractions (Frs. C1−20).

Fr. C7 (340 mg) was separated on Sephadex LH-20 CC (50% MeOH/H_2O) to obtain 16 additional fractions (Frs. C7a−p). Then Fr. C7m (70 mg) purified by semi-preparative HPLC on phenyl-hexyl column (2.0 mL/min, 29% MeCN, *v*/*v* 0.02% formic acid) to yield **5** (9 mg, t_R = 32 min), **14** (9 mg, t_R = 27 min) and Fr. C7o (37 mg) purified by semi-preparative HPLC on C18 column (2.0 mL/min, MeCN/H_2O, 36%, *v*/*v* 0.02% formic acid) to yield **17** (4.4 mg, t_R = 26 min).

Fr. C9 (888 mg) was separated on Sephadex LH-20 CC (50% MeOH/H_2O) to obtain 11 additional fractions (Frs. C9a−k). Fr. C9b (590 mg) was further purified by semi-preparative HPLC on C18 column eluted with 44% MeOH/H_2O (*v*/*v*, 0.02% formic acid) at a flow rate of 5.0 mL/min to yield **39** (150 mg, t_R = 73.0 min).

Fr. C10 (440 mg) was subjected to a Sephadex LH-20 CC eluted with MeOH to yield 6 subfractions (Frs. C10a−f), based on TLC analysis. Fr. C10a (43 mg) was purified by semi-preparative HPLC on C18 column eluted with 37% MeCN/H_2O (*v*/*v*, 0.02% formic acid) at a flow rate of 2.0 mL/min to yield **38** (7.7 mg, t_R = 17.0 min).

Fr. C11 (67 mg) was further purified by semi-preparative HPLC on C18 column eluting with 35% MeCN/H_2O (*v*/*v*, 0.02% formic acid) at a flow rate of 2.0 mL/min to yield **11** (2.2 mg, t_R = 23.0 min), **12** (15.5 mg, t_R = 26.0 min), **37** (20 mg, t_R = 11.0 min), respectively.

Fr. C12 (1.24 g) was separated on a Sephadex LH-20 CC (MeOH) to obtain 15 additional fractions (Frs. C12a−o) and then Fr. C12j (154 mg) purified by semi-preparative HPLC on C18 column (5.0 mL/min, 54% MeOH/H_2O, *v*/*v* 0.02% formic acid) to yield **25** (48.2 mg, t_R = 54.0 min), **35** (2.2 mg, t_R = 95.0 min). Fr. C12k (88 mg) purified by semi-preparative HPLC on C18 column (2.0 mL/min, 38% MeCN/H_2O, *v*/*v* 0.02% formic acid) to yield **26** (36 mg, t_R = 36.5 min). Fr. C12l (33 mg) purified by semi-preparative HPLC on C18 column (2.0 mL/min, 41% MeCN/H_2O, *v*/*v* 0.02% formic acid) to yield **28** (9.8 mg, t_R = 41 min). Fr. C12n (33 mg) purified by semi-preparative HPLC on C18 column (2.0 mL/min, 42% MeCN/H_2O, *v*/*v* 0.02% formic acid) to yield **27** (4.1 mg, t_R = 44 min).

Fr. C13 (1.15 g) was applied to a Sephadex LH-20 column eluted with MeOH to give 11 subfractions (Frs. C13a−k), based on TLC analysis. Then Subfraction Fr. C13f (45 mg) was purified by semi-preparative HPLC on C18 column eluted with 42% MeCN/H_2O (*v*/*v*, 0.02% formic acid) at a flow rate of 2.0 mL/min to yield **19** (1.0 mg, t_R = 19.0 min). Fr. C13g (247 mg) was purified by semi-preparative HPLC on phenyl-hexyl column eluted with MeCN/H_2O (2.0 mL/min, 47% MeCN/H_2O, *v*/*v* 0.02% formic acid) to yield **10** (10.2 mg, t_R = 27 min), **16** (11.7 mg, t_R = 35 min).

Fr. C14 (1.0 g) was subjected to a Sephadex LH-20 column eluted with MeOH to give 14 subfractions (Frs. C14a−n), based on TLC analysis. Fr. C14l (120 mg) was further separated by Sephadex LH-20 CC eluted with MeOH to give 6 subfractions (Frs. C14l1−6). Fr. C14l4 (29 mg) was purified by semi-preparative HPLC on C18 column (2.0 mL/min, 45%−48% MeCN/H_2O 40 min, 48%−60% MeCN/H_2O 10 min, *v*/*v* 0.02% formic acid) to yield **24** (3.5 mg, t_R = 15 min). Fr. C14l6 (12 mg) was purified by semi-preparative HPLC on C18 column (2.0 mL/min, 46% MeCN/H_2O, *v*/*v* 0.02% formic acid) to yield **22** (8.0 mg, t_R = 34 min).

Fr. C15 (483 mg) was applied to Sephadex LH-20 CC eluted with MeOH to obtain eight subfractions (Frs. C15a−h). Fr. C15f (75 mg) was purified by semi-preparative HPLC on phenyl-hexyl column (2.0 mL/min, 46% MeCN/H_2O, *v*/*v* 0.02% formic acid) to yield **31** (3.5 mg, t_R = 33 min), **33** (3.0 mg, t_R = 39 min), and **32** (16.4 mg, t_R = 43 min).

Fr. C17 (293 mg) was subjected to Sephadex LH-20 CC eluted with MeOH to get 6 subfractions (Frs. C17a−f). Fr. C17d (41 mg) was purified by semi-preparative HPLC on phenyl-hexyl column (2.0 mL/min, 50% MeCN/H_2O, *v*/*v* 0.02% formic acid) to yield **29** (3.9 mg, t_R = 41 min) and **30** (6.2 mg, t_R = 52 min).

Fr. C18 (481 mg) was further separated by Sephadex LH-20 CC eluted with MeOH to obtain eight subfractions (Frs. C18a−h). Fr. C18f (42 mg) was purified by semi-preparative HPLC on phenyl-hexyl column (2.0 mL/min, 53% MeCN/H_2O, *v*/*v* 0.02% formic acid) to yield **21** (11.2 mg, t_R = 43 min) and **23** (4.4 mg, t_R = 33 min). Fr. C18g (22 mg) was purified by semi-preparative HPLC on phenyl-hexyl column (2.0 mL/min, 55% MeCN/H_2O, *v*/*v* 0.02% formic acid) to yield **34** (1.5 mg, t_R = 27 min).

Fr. C20 (275 mg) was purified by semi-preparative HPLC on phenyl-hexyl column (2.0 mL/min, 60% MeCN/H_2O, *v*/*v* 0.02% formic acid) to yield **20** (13 mg, t_R = 47 min).

Fr. D (2.0 g) was applied to Sephadex LH-20 CC eluted with MeOH to obtain 14 subfractions (Frs. D1−14). Fr. D7 (80 mg) was purified by semi-preparative HPLC on phenyl-hexyl column (2.0 mL/min, 47% MeCN/H_2O, *v*/*v* 0.02% formic acid) to yield **4** (4.0 mg, t_R = 31 min), **7** (0.9 mg, t_R = 24 min), and **13** (0.9 mg, t_R = 26 min). Fr. D12 (80 mg) was purified by semi-preparative HPLC on phenyl-hexyl column (2.0 mL/min, 48% MeCN/H_2O, *v*/*v* 0.02% formic acid) to yield **36** (2.0 mg, t_R = 31 min).

*4.6.1. Dangelone A (**4**)*
Yellow powder $[\alpha]_D^{20}$ −181.3 (*c* 0.8, MeOH); UV (MeOH) λ_{max} (logε) 215 (4.28), 265 (4.03), 346 (4.21) nm. IR (KBr) ν_{max} 3355, 2918, 1645, 1583, 1447, 1255, 1204, 1169, 1104, 962, 797 cm^{-1}; CD (MeOH) λ_{max} (ε): 227 (−3.29), 259 (+0.49), 275 (−0.31), 306 (+0.57), 360 (−1.61) nm. ^1H NMR (800 MHz, in DMSO-d_6) and ^{13}C NMR (200 MHz, in DMSO-d_6), Tables S4 and S5. ESI-MS *m/z* 387.16 $[M+H]^+$ and 385.34 $[M-H]^-$. HRESIMS: 387.1438 $[M+H]^+$, Calcd. for $C_{21}H_{23}O_7$, 387.1438.

*4.6.2. Dangelone B (**5**)*
Yellow powder $[\alpha]_D^{20}$ −132.6 (*c* 0.4, MeOH); UV (MeOH) λ_{max} 211, 262, 346 nm. IR (KBr) ν_{max} 3305, 2978, 1649, 1585, 1456, 1257 cm^{-1}; CD (MeOH) λ_{max} (ε): 226 (−7.4), 249 (+0.98), 272 (−1.45), 307 (+0.71), 359 (−3.76) nm. ^1H NMR (800 MHz, in DMSO-d_6) and ^{13}C NMR (200 MHz, in DMSO-d_6), Tables S4 and S5. ESI-MS *m/z* 403.38 $[M+H]^+$ and 401.32 $[M-H]^-$. HRESIMS: 403.1387 $[M+H]^+$, Calcd. for $C_{21}H_{23}O_8$, 403.1387.

*4.6.3. Dangelone C (**6**)*
Yellow powder $[\alpha]_D^{20}$ −173.7 (*c* 0.8, MeOH); UV (MeOH) λ_{max} (logε) 215 (4.14), 265 (3.96), 347 (4.10) nm. IR (KBr) ν_{max} 3295, 2917, 1649, 1591, 1257 cm^{-1}; CD (MeOH) λ_{max} (ε): 230 (−2.0), 255 (+0.91), 275 (−0.27), 358 (−1.63) nm. ^1H NMR (800 MHz, in DMSO-d_6) and ^{13}C NMR (200 MHz, in DMSO-d_6), Tables S4 and S5. ESI-MS *m/z* 417.17 $[M+H]^+$ and 415.23 $[M-H]^-$. HRESIMS: 417.1190 $[M+H]^+$ Calcd. for $C_{21}H_{21}O_9$, 417.1180.

*4.6.4. Dangelone D (**7**)*
Yellow powder $[\alpha]_D^{20}$ +52.9 (*c* 0.3, MeOH); UV (MeOH) λ_{max} 215, 263, 349 nm. IR (KBr) ν_{max} 3386, 2934, 1716, 1647, 1619, 1585, 1447, 1381, 1255, 1202, 1171, 1054 cm^{-1}; CD (MeOH) λ_{max} (ε): 210 (+2.27), 225 (−0.35), 258 (+1.92), 301 (−3.95), 331 (+1.63), 361 (+1.51) nm. ^1H NMR (600 MHz, in acetone-d_6) and ^{13}C NMR (150 MHz, in acetone-d_6), Tables S4 and S5. ESI-MS *m/z* 445.22 $[M+H]^+$ and 443.38 $[M-H]^-$. HRESIMS: 467.1328 $[M+Na]^+$, Calcd. for $C_{23}H_{24}O_9Na$, 467.1313.

*4.6.5. Dangelone E (**8**)*
Yellow powder $[\alpha]_D^{20}$ +43.1 (*c* 1.4, MeOH); UV (MeOH) λ_{max} (logε) 214 (4.03), 268 (3.77), 314 (3.87) nm. IR (KBr) ν_{max} 3325, 2918, 1712, 1644, 1588, 1449, 1255, 1168 cm^{-1}; CD (MeOH) λ_{max} (ε): 230 (−1.52), 266 (+2.67), 296 (−1.11), 320 (+1.72), 352 (+1.38) nm. ^1H NMR (600 MHz, in acetone-d_6) and ^{13}C NMR (150 MHz, in acetone-d_6), Tables S4 and S5. ESI-MS *m/z* 419.17 $[M+H]^+$, 417.21 $[M-H]^-$. HRESIMS: 419.1352 $[M+H]^+$, Calcd. for $C_{21}H_{23}O_9$, 419.1337.

*4.6.6. Dangelone F (**9**)*
Yellow powder $[\alpha]_D^{20}$ +60.7 (*c* 1.9, MeOH); UV (MeOH) λ_{max} (logε) 215 (4.13), 266 (3.92), 308 (3.85) nm. IR (KBr) ν_{max} 3363, 2975, 1696, 1645, 1450, 1259, 1204 cm^{-1}; CD (MeOH) λ_{max} (ε): 212 (+1.87), 254 (+1.95), 288 (−2.11), 320 (+2.21), 374 (−0.18) nm. ^1H NMR (600 MHz, in acetone-d_6) and ^{13}C NMR (150 MHz, in acetone-d_6), Tables S4 and S5. ESI-MS *m/z* 441.16 $[M+Na]^+$ and 417.26 $[M-H]^-$. HRESIMS: 441.1138 $[M+Na]^+$, Calcd. for $C_{21}H_{22}O_9Na$, 441.1156.

*4.6.7. Dangeloside A (**18**)*
Light yellow powder $[\alpha]_D^{20}$ −52.9 (*c* 0.2, MeOH); UV (MeOH) λ_{max} (logε) 206 (4.04), 264 (3.51), 346 (3.02) nm. IR (KBr) ν_{max} 3383, 2920, 1647, 1614, 1419, 1257, 1203 cm^{-1}; CD (MeOH) λ_{max} (ε): 209 (−3.65), 232 (−0.46), 255 (+1.07), 276 (−0.45), 305 (+0.64), 358 (−2.58) nm. ^1H NMR (600 MHz, in acetone-d_6) and ^{13}C NMR (150 MHz, in acetone-d_6), Table S6. ESI-MS *m/z* 549.17 $[M+H]^+$ and 547.23 $[M-H]^-$. HRESIMS: 571.1429 $[M+Na]^+$, Calcd. for $C_{26}H_{28}O_{13}Na$, 571.1422.

*4.6.8. Dangeloside B (**19**)*
Light yellow powder $[\alpha]_D^{20}$ +134.5 (*c* 0.6, MeOH); UV (MeOH) λ_{max} (logε) 214 (3.73), 262 (3.42), 348 (3.55) nm. IR (KBr) ν_{max} 3409, 2924, 1722, 1650, 1582, 1453, 1257, 1051 cm^{-1}; CD (MeOH) λ_{max} (ε): 214 (+5.25), 262 (+5.37), 305 (−2.29), 372 (+4.04) nm. ^1H NMR (500 MHz, in CD_3OD) and ^{13}C NMR (125 MHz, in CD_3OD), Table S6. ESI-MS *m/z* 519.17 $[M+H]^+$ and 517.23 $[M-H]^-$. HRESIMS: 519.1868 $[M+H]^+$, Calcd. for $C_{26}H_{31}O_{11}$, 519.1861.

*4.6.9. Didangelone A (**20**)*
Yellow powder $[\alpha]_D^{20}$ −299.4 (*c* 0.2, MeOH); UV (MeOH) λ_{max} (logε) 216 (4.53), 267 (4.43), 300 (4.22), 361 (4.25) nm. IR (KBr) ν_{max} 3367, 2918, 1716, 1620, 1587, 1449, 1262, 1169 cm^{-1}; CD (MeOH) λ_{max} (ε): 216 (−5.56), 262 (+9.64), 295 (+11.63), 352 (+8.52), 402 (−8.35) nm. ^1H NMR (500 MHz, in CD_3OD) and ^{13}C NMR (125 MHz, in CD_3OD), Tables S7 and S9. ESI-MS *m/z* 777.44 $[M+H]^+$ 775.41 $[M-H]^-$. HRESIMS: 777.2205 $[M+H]^+$, Calcd. for $C_{43}H_{37}O_{14}$, 777.2178.

*4.6.10. Didangelone B (**21**)*
Yellow powder $[\alpha]_D^{20}$ −226.2 (*c* 0.2, MeOH); UV (MeOH) λ_{max} (logε) 215 (4.56), 267 (4.43), 299 (4.22), 360 (4.24) nm. IR (KBr) ν_{max} 3349, 3249, 2928, 2854, 1716, 1613, 1442, 1262, 1165 cm^{-1}; CD (MeOH) λ_{max} (ε): 215 (−2.08), 262 (+6.57), 295 (+10.50), 328 (−3.76), 356 (+3.99), 404 (−5.42) nm. ^1H NMR (500 MHz, in CD_3OD) and ^{13}C NMR (125 MHz, in CD_3OD), Tables S7 and S9. ESI-MS *m/z* 793.29 $[M+H]^+$ and 791.74 $[M-H]^-$. HRESIMS: 793.2121 $[M+H]^+$, Calcd. for $C_{43}H_{37}O_{15}$, 793.2127.

*4.6.11. Didangelone C (**22**)*
Yellow powder $[\alpha]_D^{20}$ −261.8 (*c* 0.9, MeOH); UV (MeOH) λ_{max} (logε) 211 (4.43), 265 (4.25), 295 (4.02), 358 (3.98) nm. IR (KBr) ν_{max} 3358, 2919, 1715, 1619, 1449, 1262, 1170 cm^{-1}; CD (MeOH) λ_{max} (ε): 221 (+2.73), 244 (−0.53), 295 (+5.30), 331 (−7.43), 389 (−4.55) nm. ^1H NMR (600 MHz, in DMSO-d_6) and ^{13}C NMR (150 MHz, in DMSO-d_6), Tables S7 and S9. ESI-MS *m/z* 809.36 $[M+H]^+$ and 807.53 $[M-H]^-$. HRESIMS: 831.1918 $[M+Na]^+$, Calcd. for $C_{43}H_{36}O_{16}Na$, 831.1896.

*4.6.12. Didangelone D (**23**)*
Red powder $[\alpha]_D^{20}$ −333.7 (*c* 1.6, MeOH); UV (MeOH) λ_{max} (logε) 208 (4.28), 266 (4.05), 301 (3.89), 364 (3.71) nm. IR (KBr) ν_{max} 3281, 2921, 1713, 1620, 1448, 1323, 1262, 1168 cm^{-1}; CD (MeOH) λ_{max} (ε): 214 (−6.24), 234 (+3.45), 295 (+16.97), 350 (+6.50), 391 (−12.70) nm. ^1H NMR (600 MHz, in CD_3OD) and ^{13}C NMR (150 MHz, in CD_3OD), Tables S7 and S9. ESI-MS *m/z* 776.34 $[M+H]^+$ and 774.45 $[M-H]^-$. HRESIMS: 776.2358 $[M+H]^+$, Calcd. for $C_{43}H_{38}NO_{13}$, 776.2338.

*4.6.13. Didangelone E (**24**)*
Red powder $[\alpha]_D^{20}$ −248.6 (*c* 0.2, MeOH); UV (MeOH) λ_{max} (logε) 215 (4.53), 267 (4.33), 300 (4.16), 363 (3.96) nm. IR (KBr) ν_{max} 3275, 2921, 1710, 1618, 1595, 1452, 1322, 1264 cm^{-1}; CD (MeOH) λ_{max} (ε): 212 (−2.33), 232 (+1.31), 296 (+6.31), 387 (−5.60) nm. ^1H NMR (600 MHz, in DMSO-d_6) and ^{13}C NMR

(150 MHz, in DMSO-d_6), Tables S7 and S9. ESI-MS *m/z* 808.30 $[M+H]^+$ and 806.49 $[M-H]^-$. HRESIMS: 808.2291 $[M+H]^+$, Calcd. for $C_{43}H_{38}NO_{15}$, 808.2295.

4.6.14. *Didangelone H (**25**)*

Yellow powder $[\alpha]_D^{20}$ −365.4 (*c* 0.5, MeOH); UV (MeOH) λ_{max} (logε) 216 (4.75), 267 (4.44), 333 (4.43) nm. IR (KBr) ν_{max} 3258, 2920, 1719, 1621, 1545, 1451, 1323, 1262 cm^{-1}; CD (MeOH) λ_{max} (ε): 232 (+14.07), 303 (+48.21), 347 (−64.22) nm. ^1H NMR (500 MHz, in CD_3OD) and ^{13}C NMR (125 MHz, in CD_3OD), Tables S8 and S9. ESI-MS *m/z* 811.40 $[M+H]^+$ and 809.38 $[M-H]^-$. HRESIMS: 811.1860 $[M+H]^+$, Calcd. for $C_{42}H_{35}O_{17}$, 811.1869.

4.6.15. *Didangelone F (**27**)*

Light yellow powder $[\alpha]_D^{20}$ −259.5 (*c* 0.3, MeOH); UV (MeOH) λ_{max} (logε) 214 (4.34), 269 (4.04), 307 (3.97) nm. IR (KBr) ν_{max} 3286, 2919, 2852, 1717, 1620, 1452, 1261, 1110 cm^{-1}; CD (MeOH) λ_{max} (ε): 223 (+10.76), 295 (+21.75), 335 (−25.94) nm. ^1H NMR (600 MHz, in CD_3OD) and ^{13}C NMR (150 MHz, in CD_3OD), Tables S8 and S9. ESI-MS *m/z* 811.41 $[M+H]^+$ and 809.34 $[M-H]^-$. HRESIMS: 811.1829 $[M+H]^+$, Calcd. for $C_{42}H_{35}O_{17}$, 811.1869.

4.6.16. *Didangelone G (**28**)*

Light yellow powder $[\alpha]_D^{20}$ −182.5 (*c* 0.8, MeOH); UV (MeOH) λ_{max} (logε) 215 (4.49), 268 (4.19), 307 (4.10) nm. IR (KBr) ν_{max} 3363, 2920, 2851, 1715, 1620, 1452, 1324, 1263, 1171 cm^{-1}; CD (MeOH) λ_{max} (ε): 211 (+7.91), 268 (+12.63), 302 (+19.28), 336 (−45.34) nm. ^1H NMR (600 MHz, in CD_3OD) and ^{13}C NMR (150 MHz, in CD_3OD), Tables S8 and S9. ESI-MS *m/z* 811.38 $[M+H]^+$ and 809.37 $[M-H]^-$. HRESIMS: 833.1708 $[M+Na]^+$, Calcd. for $C_{42}H_{34}O_{17}Na$, 833.1688.

4.6.17. *Tridangelone A (**29**)*

Yellow powder $[\alpha]_D^{20}$ −102.1 (*c* 0.4, MeOH); UV (MeOH) λ_{max} (logε) 214 (4.54), 268 (4.29), 305 (4.16), 346 (4.01) nm. IR (KBr) ν_{max} 3357, 3288, 2917, 1715, 1626, 1449, 1323, 1262, 1169 cm^{-1}; CD (MeOH) λ_{max} (ε): 227 (+16.86), 255 (−0.33), 295 (+26.64), 342 (−31.29) nm. ^1H NMR (600 MHz, in DMSO-d_6) and ^{13}C NMR (150 MHz, in DMSO-d_6), Tables S10 and S11. ESI-MS *m/z* 1205.38 $[M+H]^+$ and 1203.54 $[M-H]^-$. HRESIMS: 1205.2882 $[M+H]^+$, Calcd. for $C_{64}H_{53}O_{24}$, 1205.2921.

4.6.18. *Tridangelone B (**30**)*

Yellow powder $[\alpha]_D^{20}$ −167.4 (*c* 1.8, MeOH); UV (MeOH) λ_{max} (logε) 214 (4.66), 268 (4.44), 305 (4.32), 347 (4.17) nm. IR (KBr) ν_{max} 3362, 2920, 2852, 1715, 1621, 1449, 1324, 1262, 1168, 1105 cm^{-1}; CD (MeOH) λ_{max} (ε): 209 (+11.07), 245 (−2.09), 306 (+27.55), 345 (−27.86) nm. ^1H NMR (600 MHz, in DMSO-d_6) and ^{13}C NMR (150 MHz, in DMSO-d_6), Tables S10 and S11. ESI-MS *m/z* 1205.43 $[M+H]^+$ and 1203.54 $[M-H]^-$. HRESIMS: 1227.2653 $[M+Na]^+$, Calcd. for $C_{64}H_{52}O_{24}Na$, 1227.2682.

4.6.19. *Tridangelone C (**31**)*

Yellow powder $[\alpha]_D^{20}$ −143.2 (*c* 0.4, MeOH); UV (MeOH) λ_{max} (logε) 205 (4.45), 269 (4.15), 308 (4.02), 349 (3.87) nm. IR (KBr) ν_{max} 3394, 2920, 2851, 1734, 1645, 1466, 1325, 1262, 1103, 801 cm^{-1}; CD (MeOH) λ_{max} (ε): 227 (+25.79), 294 (+33.52), 340 (−39.96) nm. ^1H NMR (600 MHz, in DMSO-d_6) and ^{13}C NMR (150 MHz, in DMSO-d_6), Tables S10 and S11. ESI-MS *m/z* 1221.33 $[M+H]^+$ and 1219.40 $[M-H]^-$. HRESIMS: 1221.2883 $[M+H]^+$, Calcd. for $C_{64}H_{53}O_{25}$, 1221.2870.

4.6.20. *Tridangelone D (**32**)*

Yellow powder $[\alpha]_D^{20}$ −203.8 (*c* 1.3, MeOH); UV (MeOH) λ_{max} (logε) 215 (4.59), 268 (4.37), 307 (4.24), 348 (4.10) nm. IR (KBr) ν_{max} 3247, 2920, 2851, 1619, 1449, 1324, 1262, 1169 cm^{-1}; CD (MeOH) λ_{max} (ε): 211 (+8.40), 246 (−1.68), 306 (+22.93), 344 (−24.60) nm. ^1H NMR (600 MHz, in DMSO-d_6) and ^{13}C NMR (150 MHz, in DMSO-d_6), Tables S10 and S11. ESI-MS *m/z* 1221.26 $[M+H]^+$ and 1219.39 $[M-H]^-$. HRESIMS: 1243.2625 $[M+Na]^+$, Calcd. for $C_{64}H_{52}O_{25}Na$, 1243.2690.

4.6.21. *Tridangelone E (**33**)*

Yellow powder $[\alpha]_D^{20}$ −191.3 (*c* 1.2, MeOH); UV (MeOH) λ_{max} (logε) 214 (4.43), 268 (4.21), 305 (4.06), 346 (3.90) nm. IR (KBr) ν_{max} 3328, 2269, 2917, 1714, 1619, 1450, 1323, 1261, 1104 cm^{-1}; CD (MeOH) λ_{max} (ε): 226 (+16.04), 258 (−0.79), 296 (+20.80), 339 (−29.02) nm. ^1H NMR (600 MHz, in DMSO-d_6) and ^{13}C NMR (150 MHz, in DMSO-d_6), Tables S10 and S11. ESI-MS *m/z* 1207.42 $[M+H]^+$ and 1205.57 $[M-H]^-$. HRESIMS: 1229.2950 $[M+Na]^+$, Calcd. for $C_{64}H_{54}O_{24}Na$, 1229.2897.

4.6.22. *Dangelone G (**34**)*

Yellow powder $[\alpha]_D^{20}$ −186.3 (*c* 0.9, MeOH); UV (MeOH) λ_{max} (logε) 216 (4.15), 262 (3.96), 301 (3.70), 355 (3.63) nm. IR (KBr) ν_{max} 3199, 2924, 2851, 1715, 1642, 1619, 1449, 1325, 1261 cm^{-1}; CD (MeOH) λ_{max} (ε): 228 (+3.62), 255 (−2.77), 300 (+4.78), 352 (−4.69) nm. ^1H NMR (600 MHz, in DMSO-d_6) and ^{13}C NMR (150 MHz, in DMSO-d_6), Table S12. ESI-MS *m/z* 563.12 $[M+H]^+$ and 561.23 $[M-H]^-$. HRESIMS: 585.1382 $[M+Na]^+$, Calcd. for $C_{30}H_{26}O_{11}Na$, 585.1367.

4.6.23. *Dangelone H (**35**)*

Yellow powder $[\alpha]_D^{20}$ −54.1 (*c* 0.9, MeOH); UV (MeOH) λ_{max} (logε) 205 (4.15), 270 (3.60), 300 (3.56) nm. IR (KBr) ν_{max} 3331, 2918, 1730, 1618, 1455, 1261, 1102 cm^{-1}; CD (MeOH) λ_{max} (ε): 217 (−2.00), 247 (+0.26), 301 (+1.30), 342 (−2.05) nm. ^1H NMR (600 MHz, in CD_3OD) and ^{13}C NMR (150 MHz, in CD_3OD), Table S12. ESI-MS *m/z* 353.25 $[M-H]^-$. HRESIMS: 353.1032 $[M-H]^-$, Calcd. for $C_{20}H_{17}O_6$, 353.1030.

4.7. *ECD calculations of compounds **9**, **18**, **20**, **25**, **27**, **28**, and **35***

Conformational analyses of compounds **9**, **18**, **20**, **25**, and **35** were performed *via* Monte Carlo searching with the MMFF94 force field using the Spartan 10 software (Wavefunction, Inc., Irvine, CA, USA). All conformers with relative energies within 9 kcal/mol were optimized for density functional theory (DFT) calculations at the B3LYP/6-31G(d) level in vacuum using the Gaussian 09 program[36]. Subsequently, the B3LYP/6-31G(d)-optimized conformers were re-optimized at the WB97XD/DGDZVP level in methanol. The WB97XD/DGDZVP harmonic vibrational frequency analyses confirmed the stability of the conformers. ECD computations for the WB97XD/DGDZVP-optimized conformers were performed using time-dependent DFT (TD-DFT) at the CAM-B3LYP/DGDZVP level in methanol. The predicted ECD spectra were simulated by the Gaussum 2.25 program[53]. The final ECD spectra were acquired on the base of the Boltzmann distribution theory and the relative Gibbs free energy (ΔG).

Conformational analyses of compounds **27** and **28** were performed in Yinfo Cloud Platform (https://cloud.yinfotek.com/) using Confab[54] with systematic algorithm at MMFF94 force field with RMSD threshold of 0.5 Å and energy window of 7 kcal/mol. The theoretical calculations were carried out using Gaussian 09[38] (Revision D.01, Gaussian Inc., Wallingford, CT, USA, 2009). At first, conformers were optimized at PM6 and HF/6-31G(d) theory levels, consecutively. Room-temperature equilibrium populations were calculated on the basis of Boltzmann distribution law and dominative conformers with the value greater than 1% were saved. The chosen conformers were finally optimized at B3LYP/6-31G(d) in gas phase. Vibrational frequency analysis confirmed the stable structures. ECD calculations were conducted in methanol with IEFPCM model using TD-DFT. Rotatory strengths for 100 excited states were calculated. The ECD spectrum was simulated using the ECD/UV analysis tool in Yinfo Cloud Platform by overlapping Gaussian functions for each transition.

4.8. *Determination of the absolute configuration of ribose moieties in compound **18***

To verify the absolute configurations of ribose moiety in **18**, a modified method based on UPLC–MS analysis was adopted, where the parent compounds were hydrolyzed to afford the sugar samples, the retention times of which were compared with those of standard sugars (D/L)[55].

Acid hydrolysis reaction: dissloving **18** (1.4 mg, each) in 1 mL HCl (1 mol/L) treated with 3 mL MeOH/H_2O (*v*/*v*, 2:1) under 70 °C for 4 h. The reaction mixture was evaporated to dry extract, and extracted three times with EtOAc after extract dissloving in 2 mL H_2O. The water layer was evaporated to afford a hydrolytic monosaccharide.

Preparation of monosaccharide derivatives: solutions of L-ribose (2.0 mg), D-ribose (2.0 mg) and hydrolytic monosaccharides (0.4 mg, each) in 1 mL pyridine were individually treated with L-cysteine methyl ester hydrochloride (2.0 mg) under 60 °C for 2 h, and then added *O*-tolyl isothiocyanate (2.0 mg) in each reaction system under 60 °C for 1 h. A blank control group was preapared at the same time.

Each reaction mixture was analyzed by UPLC–MS. As shown in Fig. S7, the retention time of hydrolyzed monosaccharide derivative was in accordance with that of D-ribose derivative. Thus, the ribose in **18** was determined as D-configuration.

4.9. *Cytotoxicity assays*

The cytotoxicities of compounds **4**−**39** against human cancer cell lines HepG-2 and MCF-7 (NCI-60, Bethesda, USA) as well as the murine microglial BV2 cell line were measured using the MTT assay according to the reported procedures[56]. Taxol was used as the positive control.

4.10. *Anti-inflammatory assays*

The anti-inflammatory activities of compounds **4**−**39** were assessed by measuring the inhibitory effects on NO production induced by lipopolysaccharide (LPS) in murine microglial BV2 cell line according to the reported procedures[56]. Curcumin was selected as the positive control (inhibitory rate 93.7 ± 2.5% at 10^{-5} mol/L). The murine microglia BV2 cell line was purchased from the Cell Culture Center at the Institute of Basic Medical Sciences, Chinese Academy of Medical Sciences and Peking Union Medical College (Beijing, China).

4.11. *Antioxidant assays*

The antioxidant activities of compounds **4**−**39** were evaluated by measuring the inhibitory rates of malondialdehyde (MDA) in rat liver microsomal lipid peroxidation induced by Fe^{2+}-cystine *in vitro* according to the reported procedures[57]. Curcumin was selected as the positive control (inhibitory rate 91.0 ± 3.2% at 10^{-4} mol/L). Rat liver microsomes are prepared from male Sprague−Dawley rats (Hua Fu Kang Bioscience, Beijing, China).

Acknowledgments

This work was supported financially by the National Key Research and Development Program of China (2018YFA0901900), the CAMS Innovation Fund for Medical Sciences (CIFMS, 2016-I2M-1-010, 2017-I2M-4-004), and Fundamental Research Funds for the Central Universities (2017PT35001). Jian Bai was supported by the Drug Innovation Major Project (2018ZX09711001-008-001). We are grateful to Jie Zhu from National Institute of Biological Sciences for part of cytotoxicity assays.

Author contributions

Qian Wei conducted most of the experiment and wrote the manuscript; Jian Bai analyzed data, elucidated the chemical structures, and wrote the manuscript; Daojiang Yan analyzed the BGCs of anzaphilones; Xiuqi Bao, Dan Zhang, Wenting Li and Xiangbing Qi performed anti-inflammatory, antioxidant assays and cytotoxicity assays; Bingyu Liu involved in NMR data analysis; Dequan Yu involved in discussion and design; Youcai Hu designed and guided the entire project and edited the manuscript.

Conflicts of interest

The authors declare no conflicts of interest.

Appendix A. Supporting information

Supporting information to this article can be found online at https://doi.org/10.1016/j.apsb.2020.07.020.

References

1. Zhang HW, Song YC, Tan RX. Biology and chemistry of endophytes. *Nat Prod Rep* 2006;**23**:753−71.
2. Nisa H, Kamili AN, Nawchoo IA, Shafi S, Shameem N, Bandh SA. Fungal endophytes as prolific source of phytochemicals and other bioactive natural products: a review. *Microb Pathog* 2015;**82**:50−9.
3. Stierle A, Strobel G, Stierle D. Taxol and taxane production by *Taxomyces andreanae*, an endophytic fungus of *Pacific yew*. *Science* 1993;**260**:214−6.
4. Rutledge PJ, Challis GL. Discovery of microbial natural products by activation of silent biosynthetic gene clusters. *Nat Rev Microbiol* 2015;**13**:509−23.
5. Gross H. Strategies to unravel the function of orphan biosynthesis pathways: recent examples and future prospects. *Appl Microbiol Biotechnol* 2007;**75**:267−77.

6. Scherlach K, Hertweck C. Discovery of aspoquinolones A−D, prenylated quinoline-2-one alkaloids from *Aspergillus nidulans*, motivated by genome mining. *Org Biomol Chem* 2006;**4**:3517−20.
7. Scherlach K, Schuemann J, Dahse HM, Hertweck C. Aspernidine A and B, prenylated isoindolinone alkaloids from the model fungus *Aspergillus nidulans*. *J Antibiot* 2010;**63**:375−7.
8. Schroeckh V, Scherlach K, Nutzmann HW, Shelest E, Schmidt-Heck W, Schuemann J, et al. Intimate bacterial-fungal interaction triggers biosynthesis of archetypal polyketides in *Aspergillus nidulans*. *Proc Natl Acad Sci* 2009;**106**:14558−63.
9. Asai T, Yamamoto T, Shirata N, Taniguchi T, Monde K, Fujii I, et al. Structurally diverse chaetophenol productions induced by chemically mediated epigenetic manipulation of fungal gene expression. *Org Lett* 2013;**15**:3346−9.
10. Hosaka T, Ohnishi-Kameyama M, Muramatsu H, Murakami K, Tsurumi Y, Kodani S, et al. Antibacterial discovery in actinomycetes strains with mutations in RNA polymerase or ribosomal protein S12. *Nat Biotechnol* 2009;**27**:462−4.
11. Mao XM, Xu W, Li D, Yin WB, Chooi YH, Li YQ, et al. Epigenetic genome mining of an endophytic fungus leads to the pleiotropic biosynthesis of natural products. *Angew Chem Int Ed* 2015;**54**:7592−6.
12. Bai J, Mu R, Dou M, Yan D, Liu B, Wei Q, et al. Epigenetic modification in histone deacetylase deletion strain of *Calcarisporium arbuscula* leads to diverse diterpenoids. *Acta pharma Sin B* 2018;**8**:687−97.
13. Zhang T, Wan J, Zhan Z, Bai J, Liu B, Hu Y. Activation of an unconventional meroterpenoid gene cluster in *Neosartorya glabra* leads to the production of new berkeleyacetals. *Acta pharma Sin B* 2018;**8**:478−87.
14. Biggins JB, Liu X, Feng Z, Brady SF. Metabolites from the induced expression of cryptic single operons found in the genome of *Burkholderia pseudomallei*. *J Am Chem Soc* 2011;**133**:1638−41.
15. Liu Y, Ding G, Li Y, Qu J, Ma S, Lv H, et al. Structures and absolute configurations of penicillactones A–C from an endophytic microorganism, *Penicillium dangeardii* Pitt. *Org Lett* 2013;**15**:5206−9.
16. Buchi G, Snader KM, White JD, Gougoutas JZ, Singh S. Structures of rubratoxins A and B. *J Am Chem Soc* 1970;**92**:6638−41.
17. Chen RD, Yan Z, Zou JH, Wang N, Dai JG, Rubratoxin C. A new nonadride derivative from an endophytic fungus *Penicillium* sp. F-14. *Chin Chem Lett* 2014;**25**:1308−10.
18. Bai J, Yan D, Zhang T, Guo Y, Liu Y, Zou Y, et al. A cascade of redox reactions generates complexity in the biosynthesis of the protein phosphatase-2 inhibitor rubratoxin A. *Angew Chem Int Ed* 2017;**56**:4782−6.
19. Yang SW, Chan TM, Terracciano J, Patel R, Patel M, Gullo V, et al. A new hydrogenated azaphilone Sch 725680 from *Aspergillus* sp. *J Antibiot* 2006;**59**:720−3.
20. Myobatake Y, Takeuchi T, Kuramochi K, Kuriyama I, Ishido T, Hirano K, et al. Pinophilins A and B, inhibitors of mammalian A-, B-, and Y-family DNA polymerases and human cancer cell proliferation. *J Nat Prod* 2012;**75**:135−41.
21. Liu Y, Yang Q, Xia G, Huang H, Li H, Ma L, et al. Polyketides with alpha-glucosidase inhibitory activity from a mangrove endophytic fungus, *Penicillium* sp. HN29-3B1. *J Nat Prod* 2015;**78**:1816−22.
22. Yang SW, Chan TM, Terracciano J, Loebenberg D, Patel M, Gullo V, et al. Sch 1385568, a new azaphilone from *Aspergillus* sp. *J Antibiot* 2009;**62**:401−3.
23. Ren J, Ding SS, Zhu A, Cao F, Zhu HJ. Bioactive azaphilone derivatives from the fungus *Talaromyces aculeatus*. *J Nat Prod* 2017;**80**:2199−203.
24. Natsume M, Takahashi Y, Marumo S. (−)-Mitorubrinic acid, a morphogenic substance inducing chlamydospore-like cells, and its related new metabolite, (+)-mitorubrinic acid B, isolated from *Penicillium funiculosum*. *Agric Biol Chem* 1985;**49**:2517−9.
25. Buechi G, White JD, Wogan GN. The structures of mitorubrin and mitorubrinol. *J Am Chem Soc* 1965;**87**:3484−9.
26. Zhu J, Porco JAJ. Asymmetric syntheses of (−)-mitorubrin and related azaphilone natural products. *Org Lett* 2006;**8**:5169−71.
27. Tabata Y, Ikegami S, Yaguchi T, Sasaki T, Hoshiko S, Sakuma S, et al. Diazaphilonic acid, a new azaphilone with telomerase inhibitory activity. *J Antibiot* 1999;**52**:412−4.
28. Hoshiko S, Sasaki T, Yaguchi T, Tabata Y, Sakuma S, Ikegami S, inventors. Meiji Seika Kaisha Ltd. and Meiji Milk Prod Co. Ltd., assignees. *New chemical compound PF1195 and its manufacturing method*. 1999 Oct 05. Japan patent JP 11269164 A.
29. Xiao Z, Lin S, Tan C, Lu Y, He L, Huang X, et al. Asperlones A and B, dinaphthalenone derivatives from a mangrove endophytic fungus *Aspergillus* sp. 16-5C. *Mar Drugs* 2015;**13**:366−78.
30. Lopes TI, Coelho RG, Yoshida NC, Honda NK. Radical-scavenging activity of orsellinates. *Chem Pharm Bull* 2008;**56**:1551−4.
31. Lee SM, Li XF, Jiang H, Cheng JG, Seong S, Choi HD, et al. Terreusinone, a novel UV-A protecting dipyrroloquinone from the marine algicolous fungus *Aspergillus terreus*. *Tetrahedron Lett* 2003;**44**:7707−10.
32. Moore RE, Emery T. Nalpha-acetylfusarinines: isolation, characterization, and properties. *Biochemistry* 1976;**15**:2719−23.
33. Middleton AJ, Cole DS, Macdonald KD. A hydroxamic acid from *Aspergillus nidulans* with antibiotic activity against *Proteus* species. *J Antibiot* 1978;**31**:1110−5.
34. Koreeda M, Harada N, Nakanishi K. Exciton chirality methods as applied to conjugated enones, esters, and lactones. *J Am Chem Soc* 1974;**96**:266−8.
35. Itabashi T, Ogasawara N, Nozawa K, Kawai KI. Isolation and structures of new azaphilone derivatives, falconensins E−G, from *Emericella falconensis* and absolute configurations of falconensins A-G. *Chem Pharm Bull* 1996;**44**:2213−7.
36. Frisch MJ, Trucks GW, Schlegel HB, Scuseria GE, Robb MA, Cheeseman JR, et al. *Gaussian 09, revision C.01*. Wallingford, CT, USA: Gaussian Inc.; 2010.
37. Gorin PAJ, Mazurek M. Further studies on the assignment of signals in ^{13}C magnetic resonance spectra of aldoses and derived methyl glycosides. *Can J Chem* 1975;**53**:1212−23.
38. Frisch MJ, Trucks GW, Schlegel HB, Scuseria GE, Robb MA, Cheeseman JR, et al. *Gaussian 09, revision D.01*. Wallingford, CT, USA: Gaussian Inc.; 2009.
39. Steyn PS, Vleggaar R. The structure of dihydrodeoxy-8-*epi*-austdiol and the absolute configuration of the azaphilones. *J Chem Soc Perkin Trans* 1976;**1**:204−6.
40. Zabala AO, Xu W, Chooi YH, Tang Y. Characterization of a silent azaphilone gene cluster from *Aspergillus niger* ATCC 1015 reveals a hydroxylation-mediated pyran-ring formation. *Chem Biol* 2012;**19**:1049−59.
41. Chen W, Chen R, Liu Q, He Y, He K, Ding X, et al. Orange, red, yellow: biosynthesis of azaphilone pigments in *Monascus* fungi. *Chem Sci* 2017;**8**:4917−25.
42. Sanchez JF, Somoza AD, Keller NP, Wang CCC. Advances in *Aspergillus* secondary metabolite research in the post-genomic era. *Nat Prod Rep* 2012;**29**:351−71.
43. Chiang YM, Szewczyk E, Davidson AD, Keller N, Oakley BR, Wang CCC. A gene cluster containing two fungal polyketide synthases encodes the biosynthetic pathway for a polyketide, Asperfuranone, in *Aspergillus nidulans*. *J Am Chem Soc* 2009;**131**:2965−70.
44. Hui Z, Qiao K, Gao Z, Meehan MJ, Li JWH, Zhao X, et al. Enzymatic synthesis of resorcylic acid lactones by cooperation of fungal iterative polyketide synthases involved in hypothemycin biosynthesis. *J Am Chem Soc* 2010;**132**:4530−1.
45. Xie X, Meehan MJ, Xu W, Dorrestein PC, Tang Y. Acyltransferase mediated polyketide release from a fungal megasynthase. *J Am Chem Soc* 2009;**131**:8388−9.
46. Zhang X, Li S. Expansion of chemical space for natural products by uncommon P450 reactions. *Nat Prod Rep* 2017;**34**:1061−89.
47. Nozaki H, Kuroda S, Watanabe K, Yokozeki K. Gene cloning of α-methylserine aldolase from *Variovorax paradoxus* and purification and characterization of the recombinant enzyme. *Biosci Biotechnol Biochem* 2008;**72**:2580−8.

48. Chiang YM, Ahuja M, Oakley CE, Entwistle R, Asokan A, Zutz C, et al. Development of genetic dereplication strains in *Aspergillus nidulans* results in the discovery of aspercryptin. *Angew Chem Int Ed* 2016;**55**:1662−5.
49. Chen L, Wu H, Liu H, Li E, Ren J, Wang W, et al. Genetic dereplication of trichoderma hypoxylon reveals two novel polycyclic lactones. *Bioorg Chem* 2019;**91**:103185.
50. Sanchez JF, Entwistle R, Hung JH, Yaegashi J, Jain S, Chiang YM, et al. Genome-based deletion analysis reveals the prenyl xanthone biosynthesis pathway in *Aspergillus nidulans*. *J Am Chem Soc* 2011;**133**:4010−7.
51. Gao SS, Li XM, Zhang Y, Li CS, Cui CM, Wang BG. Comazaphilones A–F, azaphilone derivatives from the marine sediment-derived fungus *Penicillium commune* QSD-17. *J Nat Prod* 2011;**74**:256−61.
52. Zhao DL, Shao CL, Zhang Q, Wang KL, Guan FF, Shi T, et al. Azaphilone and diphenyl ether derivatives from a gorgonian-derived strain of the fungus *Penicillium pinophilum*. *J Nat Prod* 2015;**78**:2310−4.
53. O'Boyle NM, Tenderholt AL, Langner KM. Cclib: a library for package-independent computational chemistry algorithms. *J Comput Chem* 2008;**29**:839−45.
54. O'Boyle NM, Vandermeersch T, Flynn CJ, Maguire AR, Hutchison GR. Confab-systematic generation of diverse low-energy conformers. *J Cheminf* 2011;**3**:8.
55. Tanaka T, Nakashima T, Ueda T, Tomii K, Kouno I. Facile discrimination of aldose enantiomers by reversed-phase HPLC. *Chem Pharm Bull* 2007;**55**:899−901.
56. Qu J, Fang L, Ren XD, Liu Y, Yu SS, Li L, et al. Bisindole alkaloids with neural anti-inflammatory activity from *Gelsemium elegans*. *J Nat Prod* 2013;**76**:2203−9.
57. Hu Y, Ma S, Li J, Yu S, Qu J, Liu J, et al. Targeted isolation and structure elucidation of stilbene glycosides from the bark of *Lysidice brevicalyx* Wei guided by biological and chemical screening. *J Nat Prod* 2008;**71**:1800−5.